-

Production and Replication of Black Diamond for use as an Antimicrobial Surface

MARIA PAGE

School of Chemistry
UNIVERSITY OF BRISTOL

This thesis is submitted in partial fulfillment of the requirements for the Honour's degree of MSci at the University of Bristol.

APRIL 2023

Supervisor: Professor Paul May
Second Assessor: Professor Wuge Briscoe
Physical and Theoretical Group

Abstract

There are growing concerns around the development of antibiotic resistance in the world today, and so new methods of fighting bacterial infection are having to be developed. This report will discuss one such method that has been studied; the use of antimicrobial surfaces to kill bacteria through a mechanical method. This idea is taken from nature, as many organisms have surfaces that are topographically spiky on a nanoscale, for example the wing of the cicada. These nanospikes have been shown to be lethal to bacteria, as they rapidly destroy them through puncturing of the cell membrane. So far a range of materials have been tested to replicate these surfaces, with the greatest success coming from black silicon and subsequently black diamond; materials with a nanoneedle topography on their surface. Black diamond is fabricated as a thin coating on the surface of black silicon, making the nanoneedles extremely rigid and strong. Black diamond has had successful results for being an antibacterial material, however the process of fabrication is costly and complicated, making it unfavourable to scale up. Therefore this study finished by looking at the potential of polymers to replicate the structure and hence the antibacterial effect of black diamond, whilst being inexpensive and relatively easy to produce. The possible molding techniques and polymer choices were discussed, and a methodology has been proposed for the first experimental tests with this aim.

Acknowledgements

I would first like to thank Gulnur Zulpukarova, from whom I have learned a lot, for all of her support and instruction throughout my project. It was a pleasure working together and sharing ideas.

I would also like to thank my supervisor Paul May for providing invaluable guidance and enthusiasm whilst directing me in my project. Furthermore, I would like to extend my thanks to Jean-Charles Eloi, Robert Harniman, James Smith, Sami Alharbi and Jude Laverock for all of their help with performing sample analysis and operating equipment.

Finally I would like to thank all members of the University of Bristol diamond group for their continued encouragement and assistance throughout the duration of my project. And thank you to Josh and Andre for solving many of my problems.

Contents

1. Introduction

1.1 Antibiotics past and present

1.1.1 Antibiotic Resistance

Bacterial growth and infections are a continual source of complication in the world of science and medicine. Since the development of the first antibiotic by Alexander Fleming in the 1920's[1] antibiotic resistance has become an increasing problem in society, especially in the last 20 years.[2] There are fears of the rapid development of antibiotic-resistant bacteria in more recent times and predictions of a post-antibiotic era ahead of us.[2,3] This is an issue that has grown out of the fact that the majority of antibacterial methods humans use are based on chemical methods of attack, meaning that through mutation and evolution, bacteria can quickly develop resistance to the chemicals they are attacked with.[4] .

The most common drug used as an antibiotic is penicillin, which kills bacteria through destruction of the cell wall. It achieves this in a chemical way, by preventing the process of peptidoglycan synthesis, which in turn results in osmotic lysis happening.[5] The ever increasing use of drugs like this to fight bacterial infection is arguably one of the reasons why antibiotic resistance is becoming increasingly problematic in the world today.

Resistance can develop through a variety of ways.[6] One of these comes from the bacteria possessing a natural way of fighting the drug, for example the ability to make an enzyme that would render the antibiotic ineffective. This is known as intrinsic resistance. Another method is acquired resistance, which is where the genetic code that combats the antibiotic is passed between bacteria through close contact or bacteriophages. The third method of antibiotic resistance, and the one that links most strongly to overuse of antibiotics being the cause, is mutational resistance. Figure 1.1 below outlines the process of mutational resistance being accelerated through the presence of antibiotics.

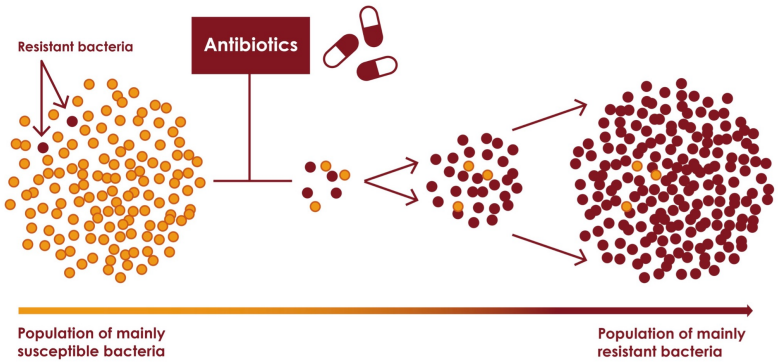

FIGURE 1.1: Scheme showing chromosomal mutation causing antibiotic resistance[7]

This process involves a specific resistant gene caused by a slight alteration to the nucleotide sequence in DNA that gives the bacteria a survival advantage, being passed down and spread through the population of bacteria, highlighted by their rapid rate of reproduction.[6] As depicted in figure 1.1 above, this results in a new resistant strain of bacteria.

The development of antibiotic resistance is creating a time-and-money-consuming cycle, in which scientists are constantly having to develop new antibiotics to treat new strains of bacteria. This is not a sustainable system, especially as each time a new antibiotic is developed, we open the opportunity for a super-resistant bacterium to evolve, that eventually could lead to a strain that is not treatable by standard methods. There is therefore an evident need to discover new methods of attacking bacteria.

1.1.2 Bacterial Growth

Bacterial infection begins with a few individual cells that could efficiently be killed with an antibiotic if treated in time, but this can often not be the case in practicality; for example if the infection is inside the body on a surgical implant. The time without treatment allows the bacterial cells to grow enough to form a biofilm, which is extremely difficult to treat with the methods we currently use. This is because once the bacteria have spent sufficient time on the surface they will multiply, creating an extracellular matrix made up of exopolysaccharides and proteins (see figure 1.2). This is called a biofilm and it acts as a barrier to antibiotics as it limits diffusion of any antibiotics through the bacterial layer, thus making it difficult for the antimicrobial agents to operate effectively. According to a study by Ceri et al, the cells are 10-500 times less likely to be killed once a biofilm has been formed.[8]

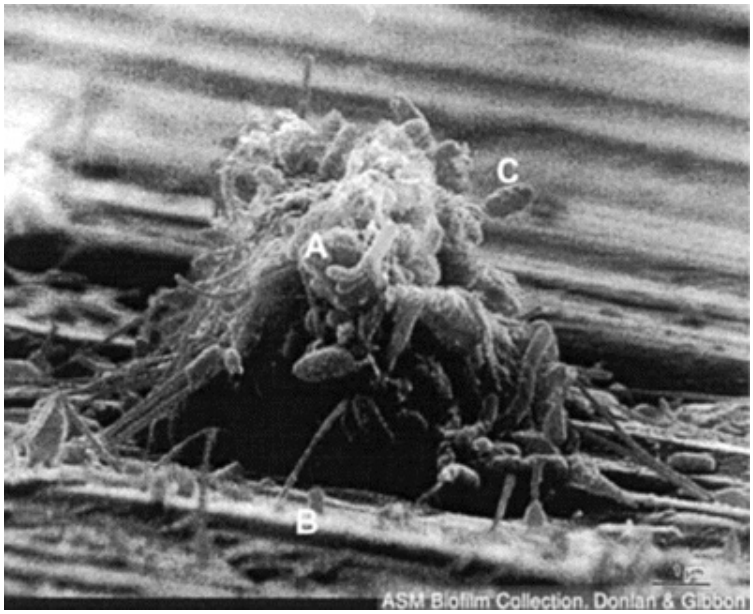

FIGURE 1.2: Biofilm formed on a surgical implant[9]

Biofouling is the name given to this process, and it results in many medical complications and is the reason why many implants have to be removed, as antibiotic treatment rarely works

against a biofilm. So in order to get around this issue and reduce the number of costly implant removal procedures that are currently necessary, antifouling surfaces have begun to be looked into. These would prevent biofilms from forming in the first place, which would provide an excellent solution to the problem outlined above.

1.1.3 Algal Growth

Biofilms can also be formed by algae. In a similar way to bacteria, algae form a layered and hard to treat coating on a surface which can lead to a range of complications in many applications in the world.[10] Current ways to deal with unwanted algal growth (for example on the bases of ships or in reservoirs) involve biocidal substances, such as copper oxides, that attack the algae in a chemical way.[11] These methods tend to be specific to each situation. This is not ideal because the problems associated with unwanted biofilm formation due to algal growth arise in a wide variety of settings. So there is no universal method that fits all situations, as the environments are so different that most bactericides can not function in all of them.

It can be seen that there is currently a gap in our knowledge and ability to fight bacterial and algal growth, as the science is being constantly 'outwitted' by the cells. It is here that antimicrobial surfaces come into play. An antimicrobial surface is one that kills cells that attempt to grow on it by a mechanical method, as opposed to a chemical one, and thus prevents biofilm formation without requiring active input from any person or chemical. This type of surface already exists in nature, with many organisms possessing their own intriguing methods of fighting bacterial infection that are effective and efficient.

1.1.4 Antibacterial surfaces in nature

There are many natural surfaces that are superhydrophobic, which is an extreme anti-wetting property that can aid antimicrobialism. This works by making it almost impossible for bacteria to attach to their surface as the adhesion forces between the bacteria and the surface are greatly reduced, due to the lack of a coating liquid medium on the surface.[12] The best known example of superhydrophobic surfaces in nature is the lotus leaf, shown below in figure 1.3.

FIGURE 1.3: Photograph of a superhydrophobic lotus leaf[13]

Any water that lands on the surface forms droplets that subsequently roll off the leaf, taking any stray bacterial cells with them.This method for preventing bacterial growth is highly effective in situations in nature, such as for the lotus leaf, but it is only effective in environments where an appropriate amount of water is present.

The cicada *(Psaltoda claripennis)* has wings which also possess antimicrobial properties.[14] It has been understood that the hydrophobic nature of this surface assists with achieving antimicrobicity.[15,16] However, further studies have been performed on the wings of cicada which have shown that it is not only the superhydrophobic effect which makes these surfaces antibacterial. As can be seen in figure 1.4, the cicada wing is covered in nanoscale needles, which are capable of destroying bacterial cells.[17]

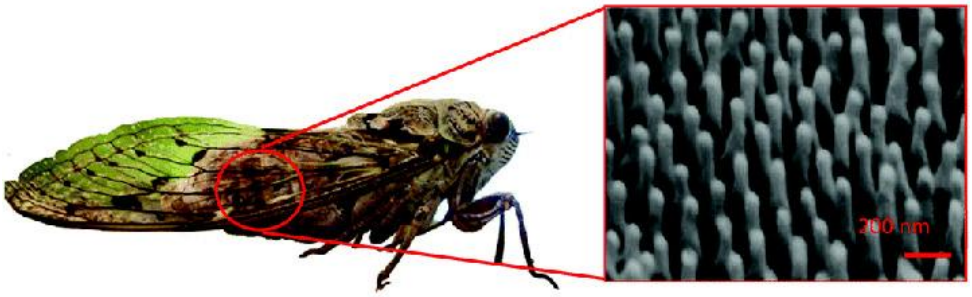

FIGURE 1.4: Photograph of a cicada, with SEM image of the nanostructured surface.[18]

A mechanism has been found and researched that demonstrates how bacteria are killed by these nanospikes; a mechanical method of achieving an antibacterial surface.[12,19] The bacterial cells are unable to survive on the surface due to the spikes which puncture the membrane of the cell and thus destroy it. This mechanism is detailed in figure 1.5. This shows in image a the initial state of the bacterium once it arrives on the surface, followed by its gradual loss of structure as the cell sinks onto the spikes (shown in images d and e) and has its membrane damaged, resulting in the death of the bacteria. This therefore prevents the formation of biofilms on the cicada wing surface, the exact effect that scientists are hoping to achieve, without the use of chemicals or need for presence of water.

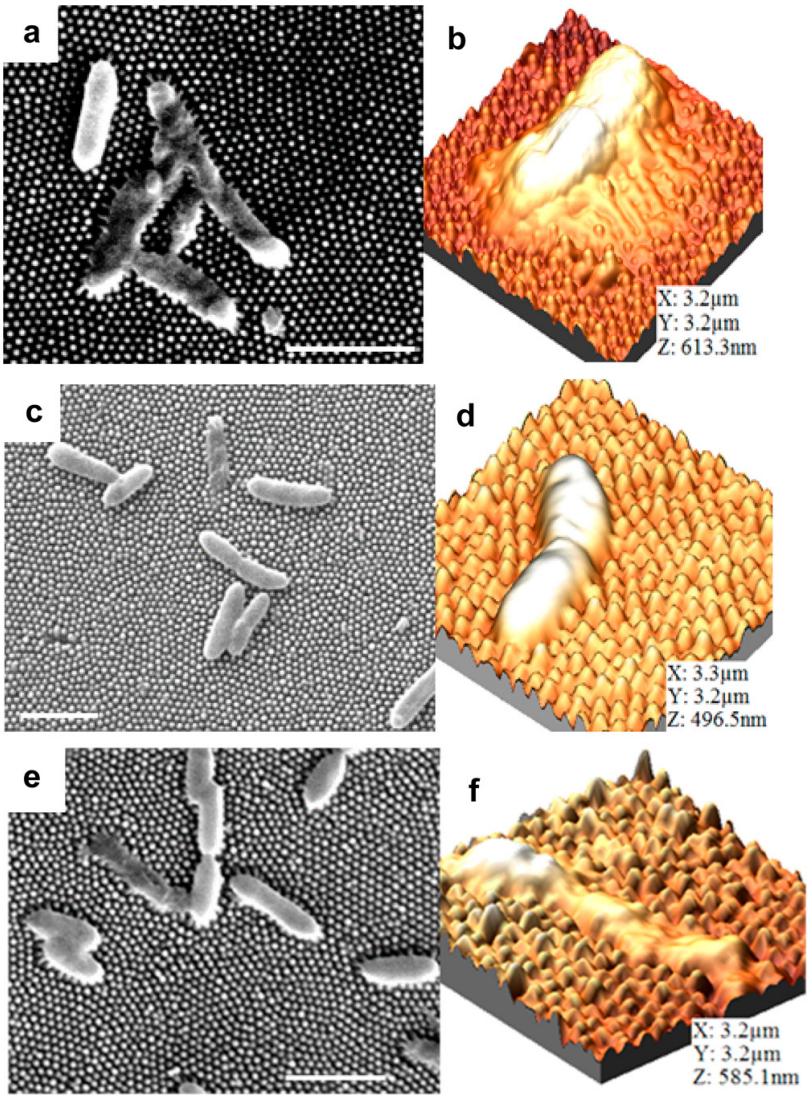

FIGURE 1.5: Scanning Electron Microscope (SEM) imagery of the process of bacterial cell death on nanopillared surfaces.[20] Images a and b show the initial state of the bacterium, while c and d show the first stage of destruction, with the cell being low down on the spikes and already losing its structure. The final images, e and f, show the bacteria completely collapsed and spread out over the spikes; the final result.

1.2 Bacterial Death

1.2.1 Antimicrobial Susceptibility Testing

There are several techniques that exist which can test the rate of death of cells on a surface. One of the most commonly used ones is live/dead staining. This involves using specifically chosen dyes that will highlight the bacteria's state either by colouring or by fluorescence. For example fluorescence staining is often carried out using SYTO9 and propium iodide.[21] Of these two dyes SYTO9 is able to cross cell membranes of any thickness and permeability, whereas the propium iodide can only cross membranes that have been damaged, and therefore can indicate a dead cell.[22] This method tends to be sensitive and produces specific results, however the high

limit for detection is a negative aspect of the method that frequently leads to an underestimation in the death rates.

Another similar method for testing bacterial death rates on a surface is one based upon enzymes. It is known as ATP bioluminescence assay. This technique operates using the luciferase enzyme which when ATP is present, will form oxyluciferin from luciferin, causing luminescence. Thus only living bacteria will emit light in this scenario. An example sample is shown in figure 1.5. This method has been used successfully in notable medical situations, for example in research into urinary tract infections.[23]

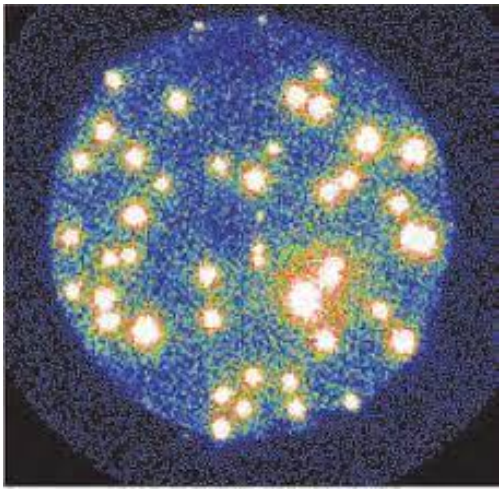

FIGURE 1.6: ATP bioluminescence assay[24]

1.2.2 Mechanism of cell destruction

In order to synthesise antibacterial surfaces, it is necessary to first fully understand the mechanism by which the cells are destroyed by the nanospikes. A report from Bandara demonstrated that the nanopillars found on the cicada wing increase the membrane deformation energy of the surface that is in contact with the bacterial membrane, thus resulting in the breaking of the membrane and death of the bacteria. This effect was tested by covering the surface in gold to ensure there was no added chemical effect that contributed to killing the bacteria.[19] This is an important step that has been taken in the majority of research into nanostructured materials because it must be clarified that the killing effect is not influenced by chemical release.[25]

The first stage of death involves the cells slowly lowering onto the spikes and their cell membranes increasingly deforming. The point of rupture was found by Tripathy et al to be after around 210 seconds, when the cells having sunk around 210 nm down onto the spikes.[26] This proposed process of death is supported by a study by Ivanova et al, the data of which are shown in figure 1.7.[19] This demonstrates a sudden change in pace of the cells sinking onto the surface needles at around 200 seconds of exposure on the surface, suggesting that there has been a significant deformation in the shape of the bacterial cell that results in the rapid falling

onto the spikes. This is called the rupture point and is demonstrated by the sudden dramatic drop in height of the bacteria cells, shown in figure 1.7.

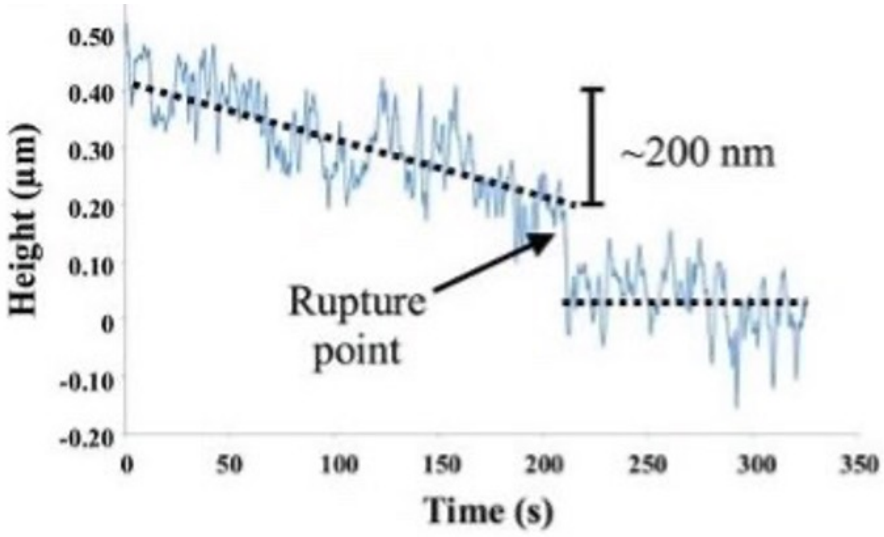

FIGURE 1.7: Graph showing the changing height of the cell of a bacterium over time as it sits on the cicada wing surface.[19]

1.2.3 Modelling cell death

Initially, little was understood about the process of cell death on the nanospikes and so Podgin et al developed a model to demonstrate a feasible scheme. In order to create a simple model that explains the process accurately, some assumptions were made. They took the membrane to be a single planar elastic membrane, given that the width of the bacterial cell membrane in relation to the diameter of the spikes is orders of magnitude greater. They also ignored the curve of the cell wall, allowing it to operate as a planar surface.[27] Figure 1.8 shows the diagram that was produced by their macroscopic model.

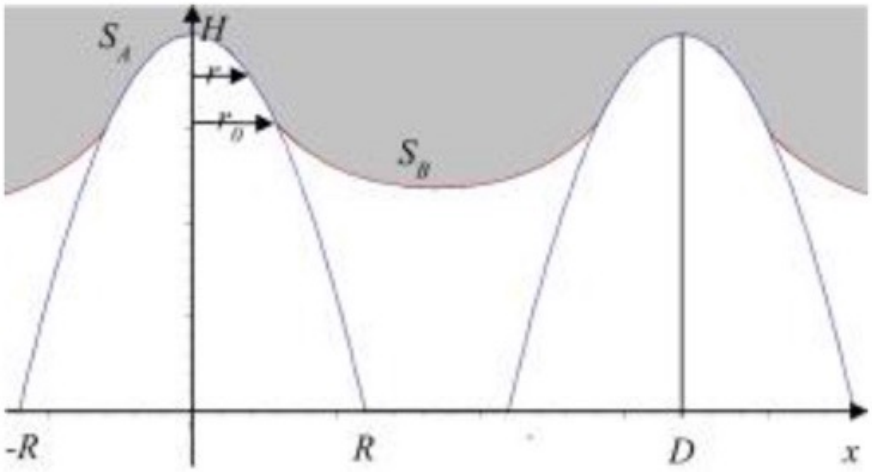

FIGURE 1.8: Cross sectional view of the deformation of bacterial cell wall on contact with nanopillared surface. The height of the nanopillar is represented by H, the bottomnwidth of the nanopillar represented by $2R$ and the distance between two nanopillars represented by D. SA is the section of the membrane in contact with the spike and SB is the section of membrane that is held between the spikes.[28]

Upon looking at the process at a macroscopic level, they showed that the membrane is stretched over the array of nanopillars, to compensate for the total surface area between the two materials increasing. This results in the membrane rupturing when it is stretched beyond its capability. This macroscale description can be combined with the molecular attractive forces at a microscale to create equations that characterise the energy lost and gained on the membrane surface.[27]

Xue et al developed some more mathematically detailed models which include factors that Podgin et al chose not to; Xue took into account the stiffness coefficent of the bacterial cell wall, using the strength of peptide bonds. This more mathematical model is accurate and detailed enough to be used to predict and suggest what will be the optimal spacing and shaping of the nanopillars, in order to obtain a high efficiency of killing.[28] This information will be useful in the future when a suitable material has been found and crafting technique developed to manufacture antimicrobial surfaces on a large scale.

1.2.4 Cell wall composition

In 1884, Hans Gram split bacteria into two different classes, known as gram-positive and gram-negative bacteria.[29] The classification is based upon the ability of bacteria to retain molecules, but for the purpose of this review, the difference in cell wall structure is the factor of importance. Gram-negative bacteria cell walls have outer and inner membranes that are joined together by lipoproteins, and the membrane is porous to hydrophilic molecules. However, for gram-positive bacteria the cytoplasmic cell membrane is about 5 times thicker than those for gram-negative bacteria, which explains why gram-negative cells are so much easier to destroy. This is also due to the layering system within the cell wall being different between the two

classes. Both types of bacteria have cell walls made up of the phosopholipid membrane and a bipolymer layer known as the peptidogycan layer which is built of two amino sugars.[30] However, these parts are put together in different ways in the two classes which ultimately results in the gram negative cell membrane being weaker. This is demonstrated below in figure 1.9.

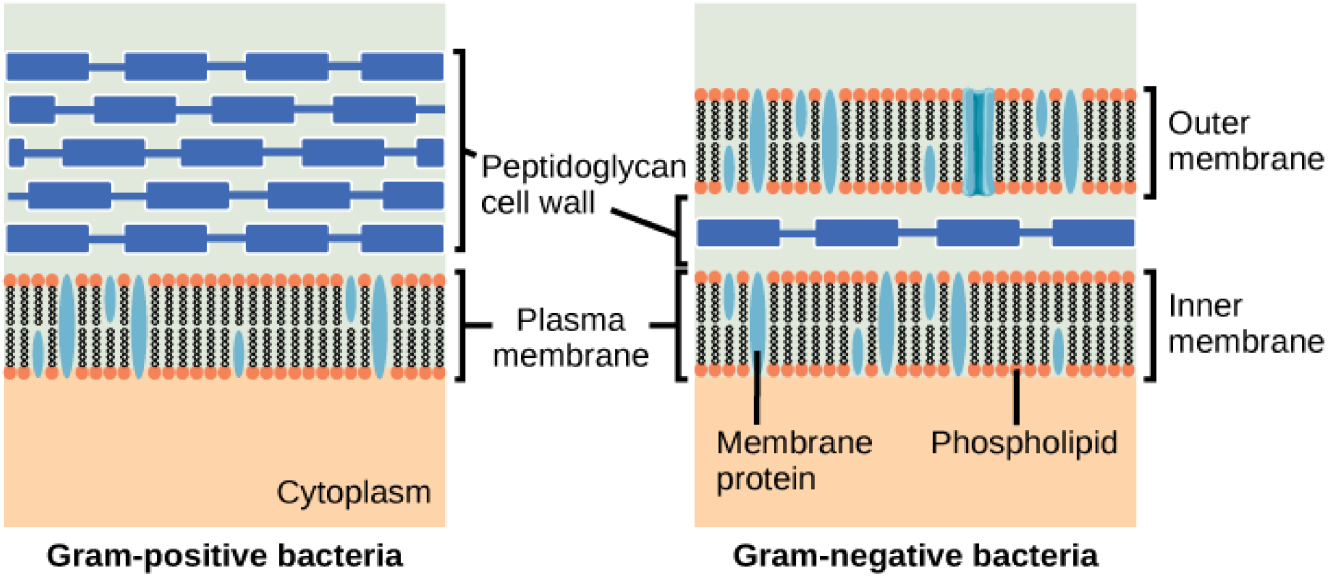

FIGURE 1.9: Simple depiction of the cell wall composition of gram negative and gram positive bacteria.[31]

On account of these structural differences, there are more reported studies of the effect of antimicrobial nanoneedled surfaces on the growth of gram-negative bacteria and fewer on gram-positive ones. This is because gram-positive cell membranes are much more difficult to puncture. However this gap in the research is being filled currently, with successful results, showing that the nanoneedles of black diamond are capable of destroying gram positive bacteria effectively as well as gram negative.

1.3 Existing Synthetic Antimicrobial Materials

1.3.1 Titanium

Titanium is one of the most commonly used medical materials, due to it having many properties that make it an excellent choice in surgical implants. One of the main problems with surgery currently is the biofilm formation and subsequent infection that can happen after an operation. So, solving this by creating a titanium surface that can be used on the implant and thus prevent bacteria from growing on it would be revolutionary in the world of medicine. Titanium surfaces that have nanospikes on have been successfully engineered, which kill bacteria by the same mechanical method as cicada wings in nature, as shown in figure 1.10.

FIGURE 1.10: SEM image of Klebsiella pneumoniae on titanium dioxide nanospikes.[32]

A hydrothermal etching process can be used to make the nanopattern on the titanium, which is a relatively inexpensive and simple process.[33] If one needs to create a more specific nanostructured pattern on titanium it is possible to use a process called Glancing Angle Deposition. This is done by firing particles of titanium at a surface from an oblique angle, which results in them building up in a highly controlled arrangement of pillars and clefts.[34] This technique is, however, much more complicated and expensive than thermal etching. This idea to make titanium surfaces antibacterial has been successful experimentally,[33,34] however much work needs to be done to consolidate the research and examine how it can be put into practice in reality.

1.3.2 Poly(ethylene glycol)(PEG) based coatings

PEG based coatings are designed to repel proteins that come close to the surface. This is achieved through the PEG surface being highly hydrophobic,[35] as well as by steric hindrance. The steric effect is due to elastic forces that are created when the PEG chains are compressed as the bacteria approaches.[36]

These types of coatings are known as polymer brushes and have been widely accepted as an effective antibacterial surface. However, the main problem with this material is that it can be oxidised in biochemical settings, which is evidently problematic as it means it is not applicable in the main environment that this research is being carried out for. Therefore it has been noted that there is a necessity to find alternative materials that are more suitable to different environments whilst achieving the same effect as PEG coatings have been proven to.[35,36]

1.3.3 Silver

Silver nanoparticles have been widely used since their properties as antimicrobial agents were discovered.[37,38]It is understood that they prevent the growth of microbes on the surface of a material, but how they do this is not yet completely known. It was discovered back at the start of using silver for antibacterial purposes in 1994 that silver reacts with the thiol groups and nucleic acids that can be found in cell walls. In this way silver disrupts the structure and composition of the cell, therefore having a similar destruction method as the puncturing caused by nanospikes in diamond. Silver ions have been shown to be able to embed themselves in proteins and cause bursting of the cells within.[39] A suggested mechanism is that the Ag forms free radicals which are able to destroy the bacteria by breaking down their membranes.[37,38] This mechanism is supported by the graph in figure 1.11, which shows an Electron Spin Resonance plot of silver nanoparticles. The two large central peaks signify the presence of free radicals, which provides the basis for the theory of destruction method outlined above.

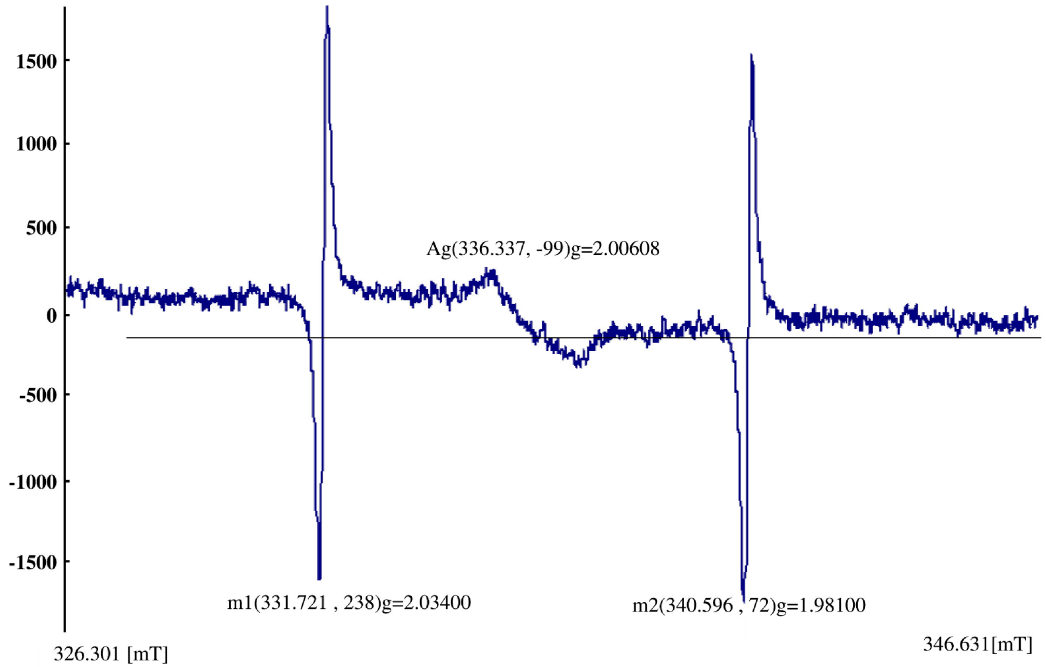

FIGURE 1.11: Electron Spin Resonance of silver nanoparticles.[37]

1.3.4 Gold

Electrodeposition has been used to tested out nanoparticular gold surfaces and their antibacterial properties. In one study from Wu et al, three types of nanostructures were tested: nanopillars, nanorings and nanonuggets, for their effect against a gram-positive bacteria that is commonly found in medical scenarios, *Staphylococcus aureus*.[40] A very good degree of success was achieved, with high death rates on all the structures, including when the surface was varied in roughness. The mechanism of death was deduced through SEM imagery to be similar to the membrane deformation effect caused on cicada wings. This approach is cost efficient and possible to upscale, but a significant drawback is that the raw materials are expensive.

1.3.5 Black silicon

Black silicon took its name due to its appearance being extremely black. This is on account of the large array of nanosized needles that it has on its surface, see figure 1.12, which absorb 99 % of light. This is because their spacing is similar to the wavelength of visible light.[41]

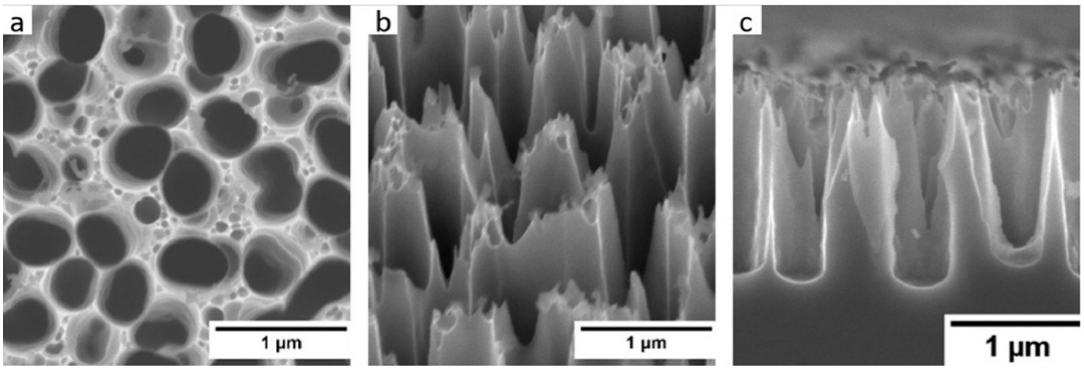

FIGURE 1.12: SEM images of black silicon surface a)vertical view, b) 45 degree view and c) Horizontal view[42]

Black silicon used to be a mere side product of reactive ion etching back in the 1980s, but due to the unique nanopillar arrangement on its surface, research into its usefulness begun in the last 25 years.[43,44] Fabricating black silicon is mostly done using a plasma and two gases. One gas does the etching of the silicon and then the second gas reacts with the new surface, creating the channels and ridges. The size and spacing of the needles can be decided during the fabrication process.[45]

An investigation was done by Ivanova et al in 2013 into the difference in topographies between black silicon, cicada wings and dragonfly wings.[19] It was found that black silicon has longer, further spaced and more spiky needles than the dragonfly wings, and that both have quite a random arrangement of pillars, which are all clustered together. In contrast to this, the cicada wing surface has an order to its distribution of spikes.[19] When they added bacterial cells to see how they reacted on the surface, the shape change was quite different on the natural surfaces compared to black silicon. But on each surface the bacteria were damaged by the nanospikes.

On black silicon and dragonfly wings the cell structures were deformed for both gram negative and gram-positive bacteria, whereas on cicada wings only gram-negative cells deformed. The rate of death was similar between all three surfaces. The important conclusion from this research and report is that all the examined nanospikes were able to kill bacteria without the necessity for a specific shape or size of needle.

The main issue with the implementation of black silicon is its fragility. It takes less than a fingernail to damage the spikes and thus destroy the antimicrobial surface.[46] This means that using black silicon on a larger scale for its antimicrobial properties would be difficult, as constant damage to the needles would be unavoidable. Thus the challenge was to find a method that would increase the strength and durability of the spikes whilst still maintaining the properties of the surface. An idea that has been explored successfully is the coating of the black silicon with a diamond layer. This adds rigidity to the surface whilst maintaining the topography and thus the bacteria destroying features.

1.3.6 Diamond

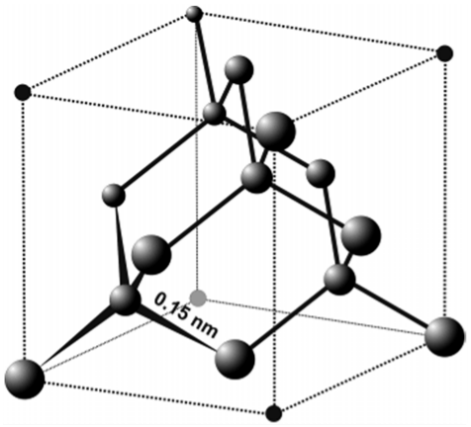

FIGURE 1.13: Structure of diamond.[47]

The sp^3 hybridised carbon atoms that make up diamond crystals are in a tetrahedral structure. Diamond itself has a range of interesting properties that hold much potential to be scientifically useful. One of these properties, and the one which is most relevant in the context of this report, arises from the strong covalent bonds (347 kJ mol^{-1}) between the carbons, make it a very mechanically hard material.[48] This material is therefore ideal for coating black silicon, as its solves the problem of the fragility of the black silicon needles by providing a layer of extreme hardness.

Black diamond is the name given to the product of coating the black silicon with a diamond layer. It is usually fabricated by the process of chemical vapour deposition (CVD) in a hot filament reactor, a method that was developed by Angus et al in the 1980s.[49] To grow diamond by CVD onto a non-diamond substrate it is necessary to seed the samples first so as to provide a

growth platform for the crystals to nucleate. The seeded substrate is then placed under vacuum in the hot filament reactor. A simplified diagram of the reactor is shown in figure 1.14.

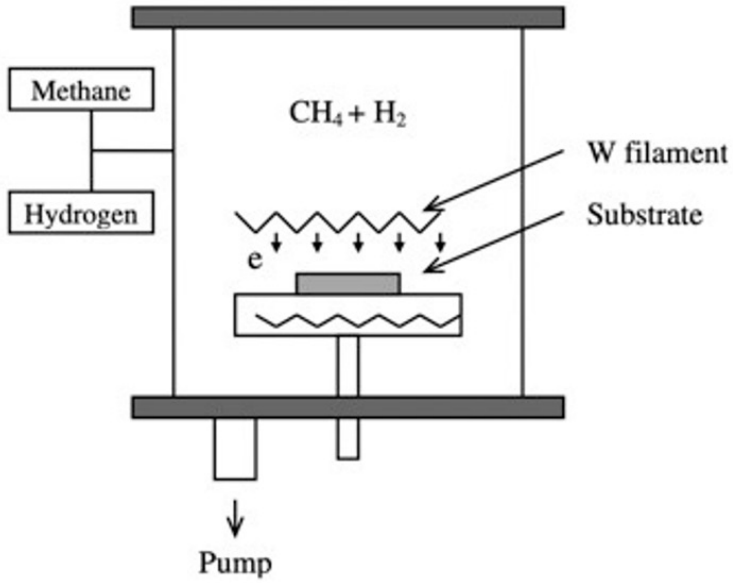

FIGURE 1.14: Schematic diagram of a hot filament CVD reactor. Once the chamber has been heated, methane and hydrogen gases are injected into it. The gases come into contact with metal filaments above the samples. These are of extremely high temperature (2200 °C) and cause dissociation of the gas molecules. The carbon-containing radicals are then free to adsorb to the surface of the black silicon below the filaments, and once there they build up over time to produce a complete layer of diamond.[50,51]

In this growing stage of the process the radicals diffuse towards the silicon surface until they come into contact with it. At this point it is possible for a reaction to occur and for the radicals to adsorb onto the surface. This happening repetitively will eventually create the desired layer of carbons that form diamond. This layer usually has extra hydrogen atoms sticking out of it, as carbons are most stable with four bonds. These extra hydrogens are removed by free hydrogen radicals, which leaves behind a reactive site on the film, that a methane radical can fill. There is the added complication that it can be a hydrogen that lands on this reactive site on the surface instead of a carbon, in which case the cycle is repeated as it has to be removed over time and replaced by a methane radical, which will form strong and irreversible covalent bonds with neighbouring carbon atoms, and thus contribute to the creation of the tetrahedal diamond lattice film.[50] This step wise reaction process is detailed in a curly arrow diagram in figure 1.15.

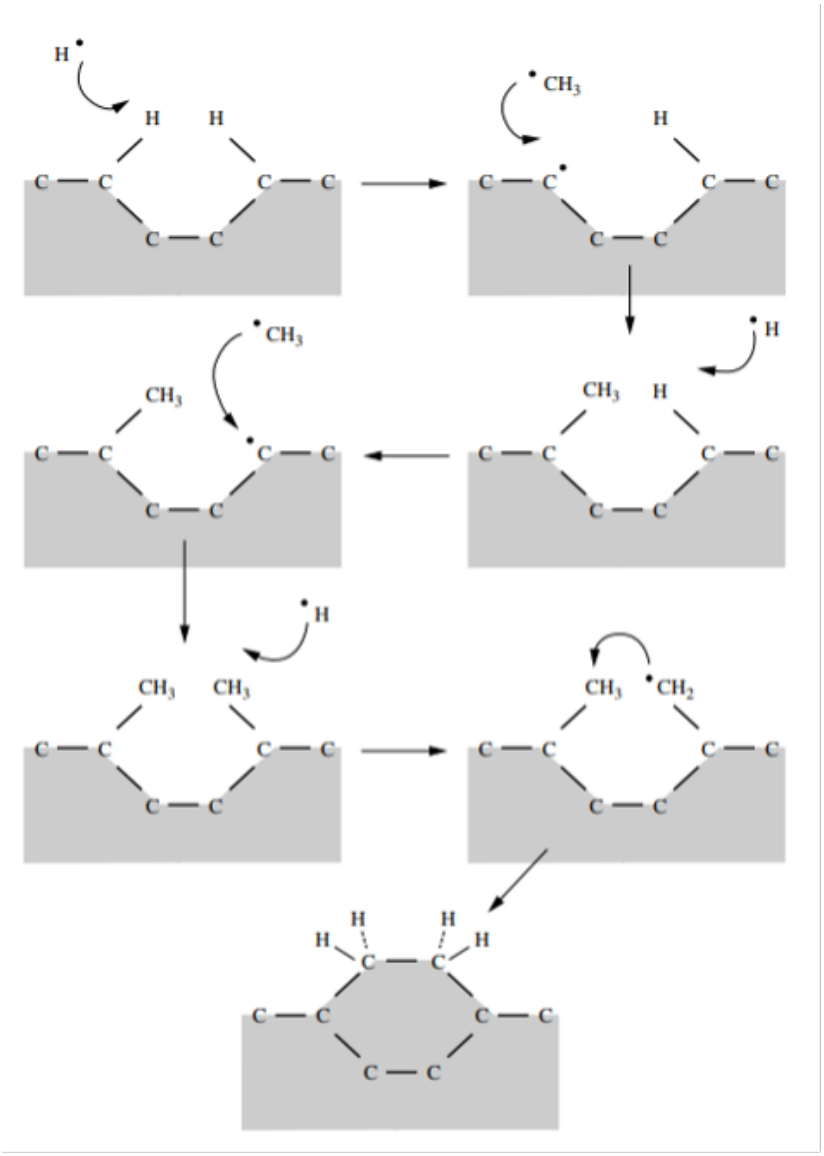

FIGURE 1.15: Diamond growth by CVD.[50]

In order to clean the surface at the end of the growing procedure only hydrogen gas is injected for two minutes, which allows the reactive atoms of hydrogen to remove any sp^2 surface carbons.

The result is a diamond-coated black silicon which has retained the topography of the black silicon needles, although there is some variation in the needle sizing and spacing. These differences are detailed in table 1.1 showing that, in general, black-diamond nanospikes tend to be shorter and wider than black silicon ones, but that the spike spacing is the same for both surfaces.

	Needle Length /μm	**Tip Radius** / nm	**Tip Separation** / μm
bSi	5-10	$\approx$ 20	$\approx$ 0.25-0.5
bD	3-4	$\approx$ 100	$\approx$ 0.25-0.5

TABLE 1.1: Differences in topography of black silicon and black diamond surfaces.[52]

These variations are not problematic as black diamond has been shown to exhibit the same antimicrobial properties as black silicon. Also, since diamond has the added benefit over black silicon of enhanced rigidity and strength, and does not oxidise in air like PEG based coatings, it is so far the superior antimicrobial surface in existence. However, black diamond synthesis is an expensive and specialist process as hot filament reactors are costly pieces of equipment with standard operating procedures. Therefore there is a need to find a material that can replicate what diamond does, without the expense, and that can be scaled up to be produced on an industrial level.

1.3.7 Applications of antimicrobial surfaces and currents issues

Antimicrobial nanostructured surfaces are still at the beginning of their discovery in the world of science and therefore there has not been enough time for research and development to make them useful on a large industrial scale. However, there have been several trials done on a materials that have other kinds of antimicrobial surfaces with successful results.[53] This implies that it will not be long before nanostructured antimicrobial surfaces will be tried too, as this technology holds evident potential for future applications.

There is however, a current concern that use of antimicrobial surfaces inside the body may end up with bacteria growing more on the body tissues around it. This risk of infection could be highly dangerous and so is a problem that will need to be overcome before it is possible to test out the new materials in implants. There is also the concern that nanoparticles may cause effects on cells that our current knowledge is not strong enough to predict. Therefore, whilst antibacterial surfaces demonstrate a huge amount of possibility for the future of fighting bacterial infection, there are hurdles to overcome before this technology can be fully implemented into industry.

1.4 The Potential of Polymers

Polymers are a material that are yet to be examined in terms of their potential in creating antimicrobial surfaces that operate like that of the cicada wing and the black diamond. The goal is to be able to develop a surface with these bacteria-killing properties that is not expensive and can be made relatively easily; and is therefore possible to scale up to an industrial level. This is where polymers would take the place of diamond.

There are two method categories for making nanoscale structures, 'top down' and bottom up'. Top down involves lithographic techniques to create the desired structures and pattern on the surface, whereas bottom up involves assembling the structure molecule by molecule. It was decided in this study to attempt the top down technique as it requires less specialist equipment.

1.4.1 Nanoimprint Lithography (NIL)

There is a technique called Nano-imprinting Lithography (NIL) that has great potential to operate well for the function outlined above.[54] This involves using heat or UV curable polymers in a two step molding process. Firstly, a flexible soft plastic would be used to create a mold, by pouring it onto the black diamond surface and then curing it. Into this soft mould would then be poured a harder plastic, which would then also be cured. Thus creating a positive copy of the original black diamond surface. The curing mechanism works due to either heat or UV activating the thermal or photoinitiator molecules and resulting in cross links forming between the polymer strands, and thus make it a rigid structure.[55] Figure 1.16 shows an outline of the NIL process. Two important benefits of the NIL process is that it is both straightforward to carry out and not expensive.

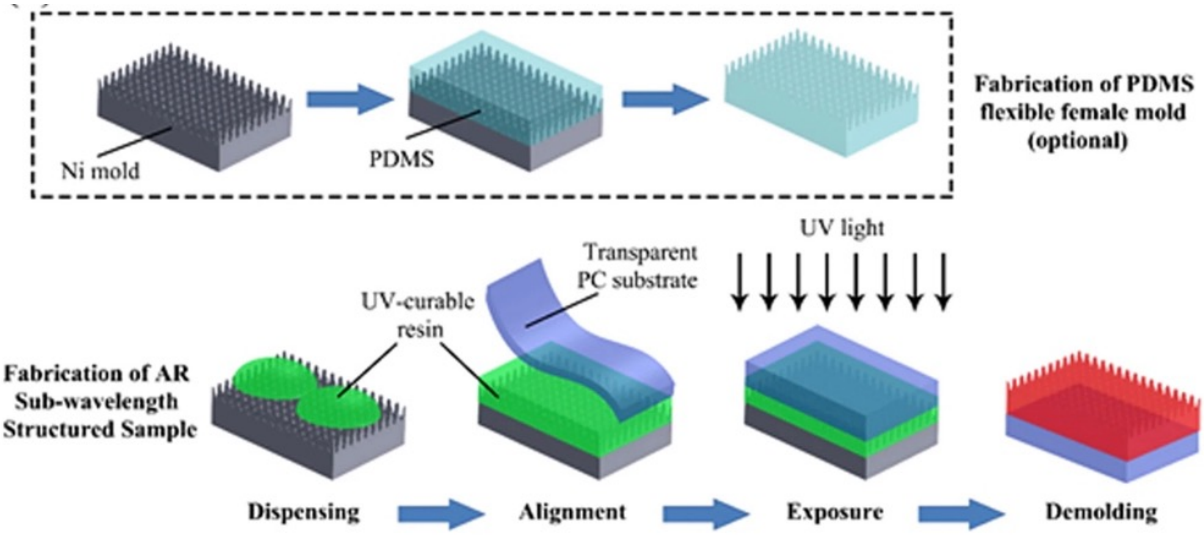

FIGURE 1.16: Schematic diagram detailing the process of NIL, using Ni as the original substrate.[55]

In order to attempt to use NIL to create a copy of the black diamond it was necessary to choose the correct polymers for their respective roles. The two requirements were a flexible polymer to pour onto the diamond and make the negative copy and a rigid polymer to be the positive copy of the initial black diamond surface.[56] The polymers chosen had to have high tensile strength (so they would not break in moulding) and be inert (so they would not react with other substances present). They also had to have a low surface energy as it was necessary to minimise attraction between the material being molded and the mold itself so that it was possible to effectively peel the layers apart. This property is related to the Young's modulus of the material. A high value means a good copy of the mold is obtained, but a low one means it is easier to remove due to less adhesion with the material. So a balance had to be struck in deciding on this aspect. The polymers also had to be able to shape into patterns of at least 100 nm diameter, as this is the scale of the topography of black diamond.

1.4.2 Flexible polymer options

Poly (dimethyl siloxane) (PDMS) is a polymer that is used widely already as a molding material and thus appeared to be a suitable choice for the flexible polymer option.[57] It is a simple siloxane heat-curable polymer that is non toxic, not flammable and inert. The smallest features that have replicated using PDMS are around 3 nm wide which makes it a small enough scale for use with black diamond which has spikes of around 100 nm diameter.[54]

PDMS is generally quite easy and safe to handle. It can be prepared for molding by mixing the elastomer base with a curing agent in a ratio of 10:1 percentage weight. Sylgard 184 Elastomer Kit can be purchased online easily, which contains the base and curing agent, and the technique for using it. The components can be mixed together using a stirring rod for 2 minutes, cleaning any spills with acetone, and then must be placed in a desiccator under vacuum for 10 minutes and then returned to atmospheric pressure. This step must be repeated until no air bubbles remain in the mixture. The PDMS can then be poured into the vesicle containing the black silicon substrate (which has been treated for anti-adhesion, see section 1.4.4) so that it covers the whole surface. It must be poured gently into the sides of the container, not directly onto the substrate, so as not to damage the surface. It must then be left to allow the cross-links to form in a closed container at room temperature for 48 hours, 100 °C for 35 minutes, 125 °C for 20 minutes or 150 °C for 10 minutes. The curing mechnism is shown below in figure 1.17. The second and third times and temperatures listed have been the most reliable in reports so far. Once cured, the PDMS can then be peeled off carefully.[58,59]

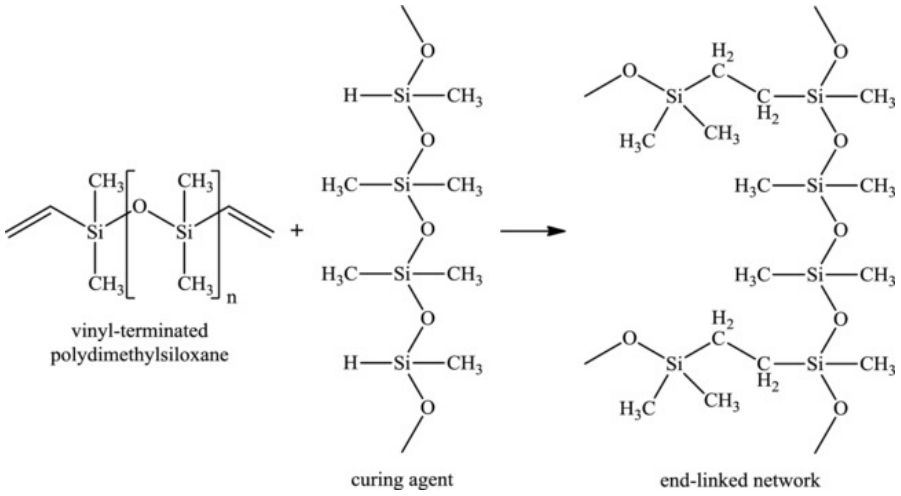

FIGURE 1.17: Curing mechanism of PDMS

There are minimal hazards to humans concerning PDMS. It has low toxicity if ingested but can be an irritant to skin and eyes. It is necessary to wash thoroughly with water if PDMS is spilled on the body. It is inflammable and inert. It is however, toxic to aquatic life so must be disposed off correctly.

If the PDMS had failed to create a quality mold, Teflon AF 2400 Tg 240 has been found to be another promising option. It has been used widely as the flexible polymer that molds onto a hard silicon surface. Looking at its surface energy as well as tensile modulus values, it fits the criteria of being able to maintain its shape whilst not adhering too strongly to the substrate. It can maintain the shape of imprinted features on a scale of as small as 80 nm whilst also molding to them and not sticking.[58] However, there have been fewer studies done using this material and therefore it was decided in this study to try out PDMS as the first attempt.

1.4.3 Rigid polymer options

Tripropylene glycol diacrylate (TPGDA) is included in a report that compares the success of four polymers in NIL. TPGDA came out the best for its fidelity in the final product pattern compared to the initial substrate.[56] TPGDA also has a high Young's modulus and therefore low adhesion to the substrate. In terms of hazards, TPGDA has low toxicity if ingested or inhaled. It can be irritant to skin and eyes so it is necessary to wash thoroughly with water if spilled. It is toxic to aquatic life and is partially biodegrabale. The process of using it as a UV resin is straightforward.[56]

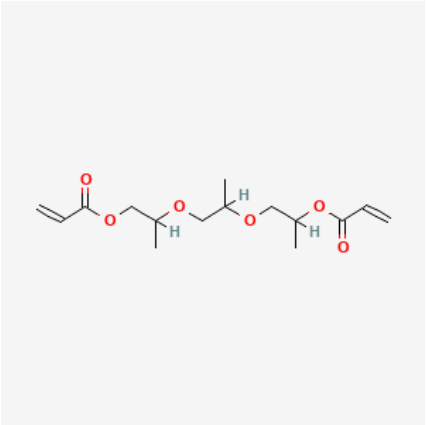

FIGURE 1.18: Structure of TPGDA

Another option for the hard polymer, should the TPGDA be ineffective is mr-NIL 6000E. This is a specific for NIL developed thermal and UV setting polymer that works as a solid resin in a NIL context. Successful resolution has been achieved on a scale of 75 nm.[60] As with the flexible polymer choice though, there has been less research done on this polymer and so it was decided to attempt with TGPDA first.

1.4.4 Anti-adhesion layer

One of the main issues faced so far with NIL is the molds binding together and being difficult to separate, which results in broken nanopillars and a failed attempt at molding. To work out the predicted adhesion between the diamond surface and the PDMS it is possible to calculate the contact angle using Young's modulus.[61] A higher contact angle means lower surface energy and therefore fewer adhesive forces will be present between the two surfaces. Zhong et al investigated the difference between using an anti-adhesive coating on silicon samples or not during the molding process.[62] It was demonstrated that an anti-adhesion layer has a significant positive effect, as shown in figure 1.19 below.

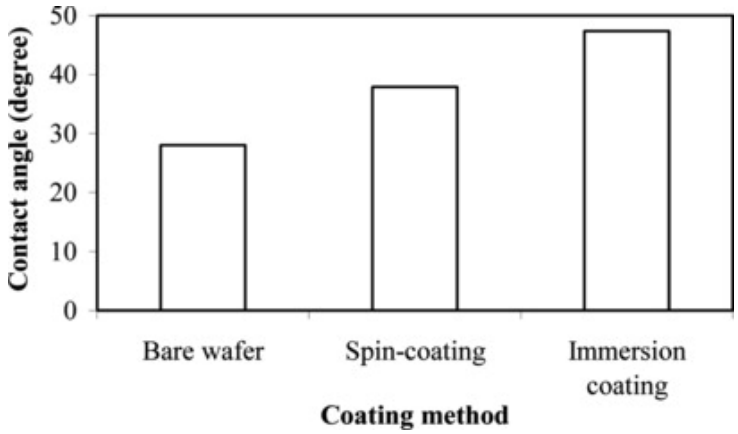

FIGURE 1.19: Results demonstrating the effect of an anti-adhesive coating (FDTS)on surface adhesion forces[62]

Given this information, it was found that there are several options that could be used to reduce the sticking between the diamond surface and the molding polymer, of which a few were selected to explore as being the most appropriate for carrying out in the Diamond Lab in Bristol.

One such method is treatment to make surfaces hydrophobic or hydrophilic, in order to add repulsive forces between the substrates.[56] It is possible to terminate the surfaces with SF_6 or Ar to make them hydrophobic, and terminating with O_2 can make them hydrophilic. However, the issue with this option is that if the substrate and the molding material are too opposite in their properties in water they will not be able to fit flush together to create the mold that we require, due to repulsive forces between them. So this method is worth trying, but it was anticipated that there would be poor molding fidelity in the results.

Another technique would be including a fluorosilane agent layer. This would increase the anti-adhesion forces between the surfaces therefore making it easier to peel them apart. Fluorosilane self assembled monolayers (F-SAMs) have been a popular choice, due to their low surface energies, when it comes to anti-adhesive coatings in NIL.[63] However, there are still imperfections in its implementation such as its lack of reusability, as well as these chemicals being hazardous to the environment; factors which make this option less favourable. It is easy to apply the layer using a liquid-phase deposition technique. These compounds work as anti-sticking layers due to the trimethyl siloxane groups, which are hydrophilic. This means that water can remove the carbon aspects from these groups, creating silanol end-groups instead. This then permits covalent bonds to form between the silanol groups and the surface of the material.[64] This proposed mechanism is shown in figure 1.20. The mechanism concerns silicon as the substrate, because the SiO_2 layer on its surface is what can bind with the silanol groups in condensation reactions. It is therefore not guaranteed to work in the same way if attempted with a black diamond surface.

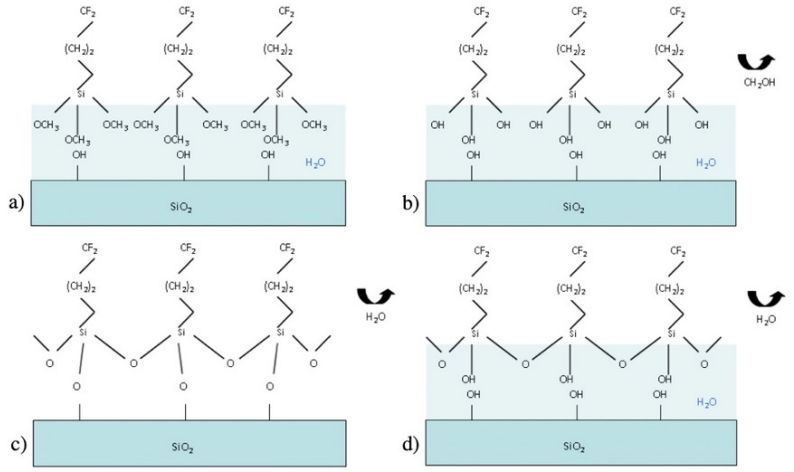

FIGURE 1.20: The effect of an anti adhesive coating (FDTS)on surface adhesion forces, showing bond formation between silanol groups and the substrate surface.[64]

This method can be modified slightly to use plasma treatment with a fluorosilane carbon layer, which is a method that has been tested with diamond surfaces. One report by Schvartzman et al looked into plasma treament using CHF_6 and C_4F_8 as the treatment plasmas.[65] This resulted in significant success at increasing the water contact angle on the material surface, and therefore making the diamond surface more hydrophobic and lower in surface energy, as demonstrated in figure 1.21.

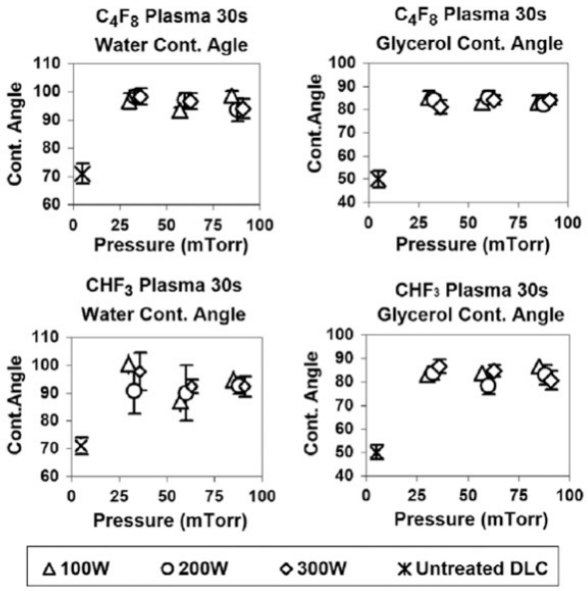

FIGURE 1.21: Water contact angle from CHF_3 and C_4F_8 plasma treated diamond surface[65]

The fluorocarbon layer reported was around 1-2 nm in thickness, which means that the nanospike topography would not be lost on account of the layer being present. Upon testing, as shown in figure 1.22 above, fluorocarbon-plasma treatment was found to be effective at decreasing the sticking between the diamond and the molding polymer, as well as still allowing a good replica of the substrate to be made.[65] Other similar studies that have examined the effect of coating diamond surfaces on the wetting properties have produced results of the same nature.[66] This is therefore a method that holds high probability to work well in the proposed research.

There is great potential in using the techniques and materials outlined above to attempt to replicate the nanostructure of black diamond in a polymer and hence develop a new antimicrobial surfaced material. By bringing together ideas from previous research and papers it has been possible to outline a possible method that holds a reasonable probability of success.

1.5 Previous Work

Antimicrobial surfaces in nature have been researched well and reliably enough to know that they hold real and exciting properties that are worth putting resources into trying to replicate. Attempts made so far to do this, using a range of materials and methods, have come up with some reasonably good methods. Black diamond so far is the most effective option that has been found. It exhibits good mechanical strength as well as efficient killing of bacterial cells on the surface. However, the main issue with black diamond is the cost and complicated nature of its fabrication, which makes it difficult to realistically envision it being used on an industrial scale.

Therefore this report marks the start of a search for a material and method that can replicate the structure and function of black diamond. It has been concluded through this review that polymers are an avenue that is yet to be pursued, but that hold promise to be successful. It has been decided that a suitable first approach to attempt is nanoimprinting lithography, a molding and demolding method that will use two different kinds of polymer and curing to end up with a positive copy of the black diamond surface. This method should ideally be relatively simple and cheap, and result in an effective and reusable antibacterial material that is easy to produce on a large scale.

1.6 Project Aims

This project aimed to produce enough samples of black diamond that were sent off to Groningen University in the Netherlands to be analysed for their effectiveness at killing gram positive bacteria. Through production of black diamond samples, the growth conditions and time were recorded and monitored, to ensure the reliability and reproducibility of the sample structures.

The second and more ambitious aim of the project was to experiment with methods and materials to try to create an antimicrobial surfaced polymer, that has the same nanoneedle structure as black diamond. The technique that was to be explored was that of nanoimprinting lithography, with poly (dimethyl siloxane) being the first polymer that would be experimented with. As this area has not been researched before, this work should hopefully set a good and exciting grounding for future research.

2. Methodology

2.1 Diamond Growth

2.1.1 Sample Preparation

Black silicon wafers were provided by LAM Technologies. A diamond tipped scribe and tweezers were then used to cut the wafers into 0.5-1 cm^2 sized squares which were suitable for use in the hot filament reactor.

2.1.2 Seeding

It was necessary to seed the black silicon prior to chemical vapour deposition in order to provide a suitable surface for the diamond to grow on through enabling nucleation. Seeding solutions were made up by diluting detonation nanodiamond (DND) of particle size 3.3 ± 0.6 nm with 2.0 weight to volume in water, in methanol. For each suspension 10 drops of DND were used with 30 ml methanol. Using an ultrasonic probe, each resulting suspension was sonicated for 3 hours. This was in order to break up any clusters of particles that may have formed. Once sonicated, the solution was poured into a petri dish, and the black silicon wafers were submerged in the suspension for one hour. They were then dried in air for 20 minutes prior to storage.

2.1.3 Diamond Growth

Diamond was grown by chemical vapour deposition in a hot filament reactor (HFCVD). Figure 2.1 below is a photograph of the hot filament reactor that was used in this study.

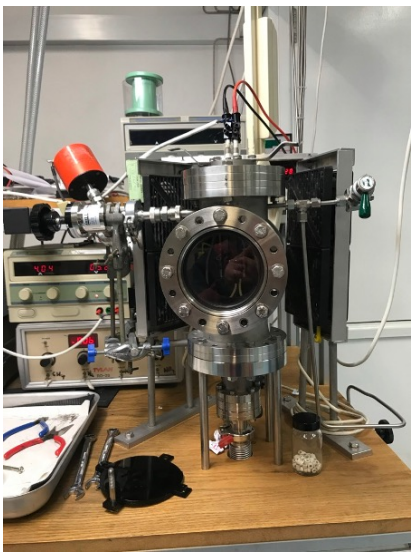

FIGURE 2.1: Hot filament reactor, University of Bristol

Either two or three seeded black silicon samples were positioned on a plate below three filaments made of tantalum wire. The samples were then placed into the reaction chamber which

was sealed and put under vacuum (at a pressure of 10^{-2} Torr). Once the vacuum was established the chamber was heated for 30 minutes, with the substrate heater delivering a current of 4 A, decreasing the pressure further to around $9{\times}10^{-2}$ Torr. Once heated, methane and hydrogen gases (1:99 ratio) were injected into the chamber at flow rates of 2 sccm for methane and 200 sccm for hydrogen. The chamber pressure was maintained at 20 Torr and then a current of 25 A applied to the filaments. The diamond was then left to grow for 20, 30 or 40 minutes, after which the methane tap was turned off, to allow the pure hydrogen to clean the surface for one minute. Then the substrate heater, filament power supply and hydrogen gas flow were turned off and the reactor allowed to cool down. Once cooled the reactor was returned to atmospheric pressure and the black diamond samples removed. Figure 2.2 shows the appearance of three black diamond samples grown in this study under the wire filaments.

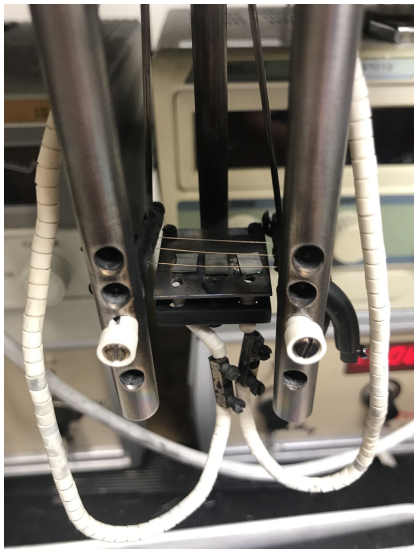

FIGURE 2.2: Black diamond samples under tantalum wire filaments, having grown for 30 minutes.

2.1.4 Termination

In order to make some of the surfaces hydrophobic they were terminated with fluorine. This was done by placing them in a DC plasma reactor. Air was then evacuated from the chamber and argon injected for ten minutes. Next the chamber was pumped down to vacuum (<10 mTorr) and then SF_6 injected in. The pressure was increased slightly to 1 Torr and then a voltage applied to the sample tray for between 5 and 10 seconds. This created a fluorine plasma above the sample surface.

2.2 Characterisation of Samples

2.2.1 Raman

A Renishaw Raman Spectrometer was used to record Raman spectra of the samples. The power of the laser was 30 mW and the wavelength of the beam was 514 nm. A variety of accumulations and spectra aquisitions were taken for each sample, to obtain the optimum spectrum. The optimum was found to be 10 aquisitions with a 5 second exposure time for silicon and 1 acquisition with 1 second exposure time for diamond.

2.2.2 Water droplet contact angle

A Kruss droplet shape analyser was used to measure the water contact angle on fluorine terminated samples to test the success of the termination by assessing the resulting hydrophobicity. The machine was first calibrated and the sample placed on the platform, in view of the side facing camera. The syringe was loaded with deionised water and then the needle was used to deposit a droplet of volume 1.5 microlitres onto the sample. The contact angle between the droplet and the surface was recorded.

2.2.3 Scanning Electron Microscopy

Samples were analysed using scanning electron microscopy, producing images which show the nanostructure of the surface. Images were taken of black silicon, black diamond and flat diamond. They were taken from top view and cross sectional view, at a variety of magnifications. The cross section were taken from samples broken in half so as to use the centre of the samples and thus avoid the potentially overgrown edges of the sample plates.

2.2.4 X-ray Photoelectron Spectroscopy

XPS was further used to determine the composition of the samples through confirmation of the presence of Si, C and F atoms in the respective materials. A photoemission electron angle of 35 $^{\circ}$ was used in order to characterise the spikes, and the sample was tilted slightly in order to improve sensitivity. These angle adjustments allows for angle resolved XPS which is ideal for the non destructive depth profiling that was carried out.

Two types of diamond samples were measured: flat and needle (black) samples. Both were mounted using carbon tape, with a strip of carbon tape attached to the top surface to assist electrical contact with the ground. Both samples were outgassed for > 4 days under ultra-high vacuum before measuring due to their high initial outgassing rates. The X-ray source used was a monochromatic Al K source (1486.7 eV) operating at 15 kV and 18 mA (270 W). The analyser was a Scienta Omicron Argus analyser.

Both samples were measured with and without a charge-neutraliser in case of charging. Charging was not noticed to be significant during the experiment. All high-resolution spectra were

recorded with aperture of 4. Survey spectra were recorded with a pass energy of 50 eV and high-resolution spectra were recorded with a pass energy of 20 eV. Angle-resolved XPS spectra were recorded with aperture of 3 and with a pass energy of 100 eV.

2.3 Polymer molding

2.3.1 Creation of a negative copy using PDMS

The molding procedure can be divided into 6 main steps: preparation of the mold by termination, scaling and mixing of the PDMS and the curing agent, degassing to remove bubbles, pouring PDMS onto the mold, baking and peeling the PDMS off the mold.

It was necessary to terminate the substrate with fluorine to make the black diamond hydrophobic in order to allow ease of separation in the later stages of the process. The F-termination stage was carried out as outlined above (see section 2.1.4)

Using a weighing cup and a scale, a mass of 10g of PDMS was weighed out and then 0.1× this mass of curing agent was added to it. After the first attempts the polymer was found to be fracturing after heat curing with this 10:1 ratio of PDMS:curing agent, as shown in figure 2.3.

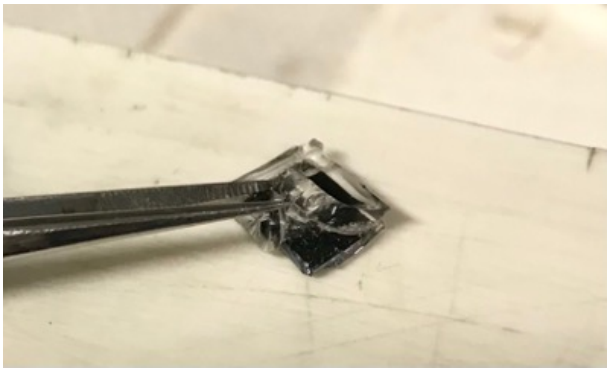

FIGURE 2.3: Photograph of PDMS fracturing when demolding, 03/03/2023

A previous study had found that the elastic forces in PDMS start to decrease when the ratio of PDMS:curing agent is higher than 9:1,[67] hence the PDMS:curing agent ratio was changed after the first round of tests to a 9:1 ratio, in an attempt to maximise elasticity of the cured PDMS. The size of the mold substrate surface determined the quantity of PDMS required. For example, for a 10/10 cm^2 surface, 40 g of PDMS resulted in a 5 mm thick resulting mold. Care was taken to account the size of the dish that the substrate was positioned in so that the PDMS liquid covered its whole surface.

Once weighed, the solution was mixed thoroughly using a plastic swab. This allowed cross links to form thus building the desired polymeric structure. The mixing process resulted in bubbles in the PDMS which had to be removed before the molding process began. One simple but effective method to do this was use of a desiccator and vacuum pump. The cup of PDMS

was placed inside the desiccator and slowly brought under vacuum. It was left for around 30 minutes and then the vacuum was gradually released and the PDMS removed. Care was taken to conduct this step slowly so as not to agitate and overflow the PDMS. The black diamond wafer was positioned in a crucible and then the PDMS was poured over. Any bubbles that appeared during this process were removed using a needle. The next step was to heat cure the PDMS, for which two different temperatures were tested. One was to place it in an oven to bake at 65°C for 2 hours, and the other was leaving it at room temperature for 48 hours. The sample was removed from the oven; its appearance is shown in figure 2.4.

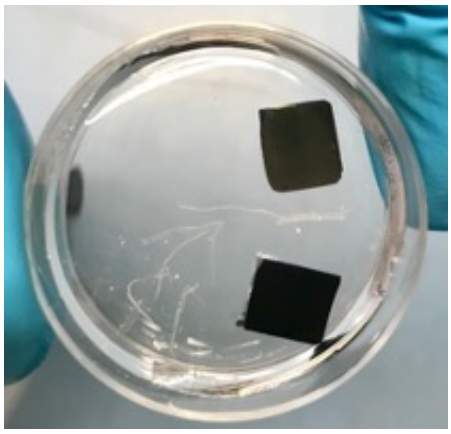

FIGURE 2.4: Photograph of PDMS poured over a black diamond and a black silicon sample, 01/03/2023

The PDMS was then peeled off the substrate using tweezers, and cut to size using a razor blade, resulting in a negative copy of the initial black diamond substrate. This step posed problems as the PDMS stuck strongly to the substrate. After the first round of tests it was therefore decided to attempt to use a lubricant as an anti-adhesion layer. The chosen lubricant was WD40 and so a second round of tests was carried out including this on the surface of the substrate. This process was repeated for a variety of substrates: black diamond, fluorine-terminated black diamond, black silicon and fluorine terminated black silicon.

2.3.2 Creation of a positive copy using TPGDA

The plan was for the TPGDA to be poured onto the prepared PDMS mold from stage 1, so that the surface was covered completely. Then a thin sheet of polymer would be placed on top of the resin to act as a support. This sheet would then be gently pushed on in order to remove any air bubbles or leftover resin solution. This structure would then be placed under a UV lamp of 1.8 W cm^{-2} for 20 seconds. After this UV curing step, the two layers would be peeled apart, resulting in the desired positive copy of the initial diamond substrate. Unfortunately, there was not enough time to carry out this proposed step to be included in this report.

3. Results and Discussion

3.1 Black Diamond

In order to verify that the black diamond samples produced in this study were as expected, it was necessary to analyse both the atomic make up of the samples and their surface topography. This was done using a variety of techniques.

3.1.1 Verification of Sample Compositions

Raman

Raman spectroscopy was used to check the sample composition, with flat and black versions of both silicon and diamond being examined.

According to the literature we can expect the second order peak in the Raman spectrum for black silicon to be in the range of 900-1100 cm^{-1}.[68] This value is different to that expected for single crystal silicon, due to the needles found on the black silicon surface scattering the laser beam.[69]A variety of acquisitions and exposure times were experimented with in order to give the smoothest resulting spectrum. In this study it was found that the best results for black silicon were obtained using an acquisition number of 10 and a 5 second exposure time. The resulting spectrum shown below in figure 3.1 has a strong peak at 946 cm^{-1}, thus in line with the literature for nanostructured silicon.

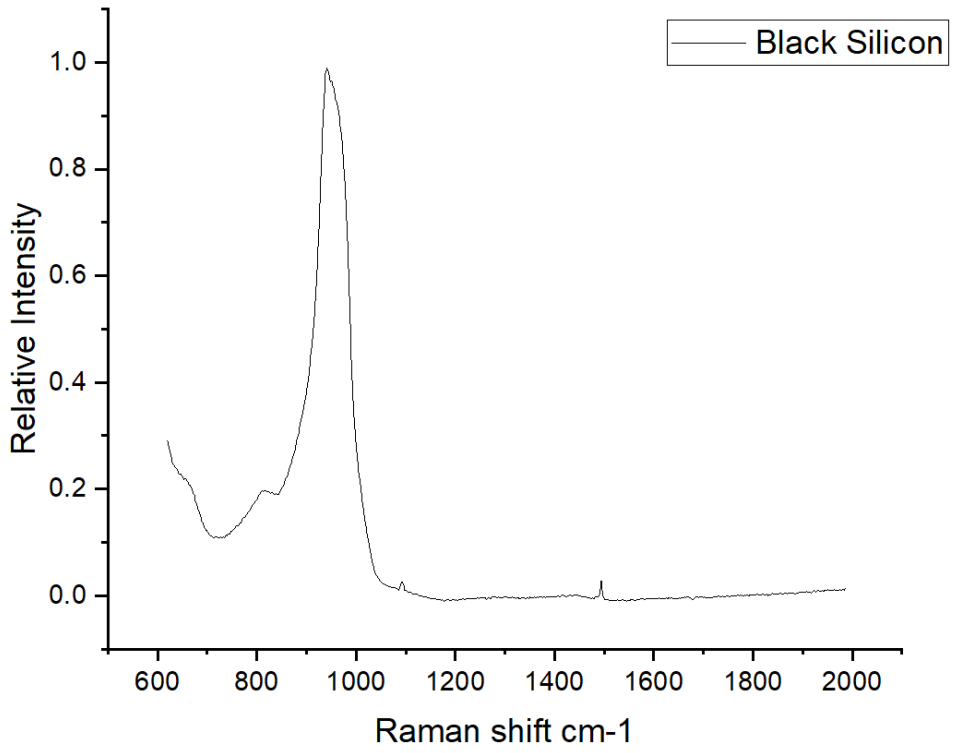

FIGURE 3.1: Black silicon Raman spectrum

In Raman spectra of crystalline diamond that are found in literature, a peak should be observed at 1332 cm^{-1}.[70] As the samples in this study all contain only a thin layer of diamond, created with a relatively short growth time, it was expected that the resulting spectra would not have as strong peaks in this region, but were hoped to at least show a significant peak. This was the case as shown below in figures 3.2 and 3.3 of black diamond and flat diamond. The intensity of this peak is affected by the purity of the diamond as well as any defects in individual crystals.These spectra were obtained using an aquisition number of 1 with a one second exposure time, with the laser power at 50%.

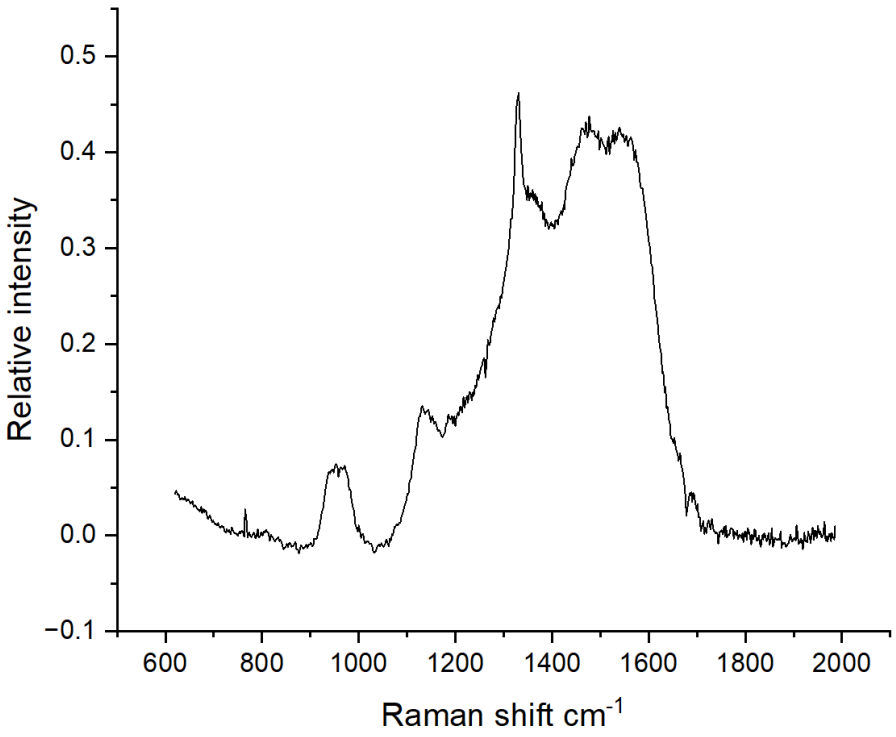

FIGURE 3.2: Black diamond Raman spectrum

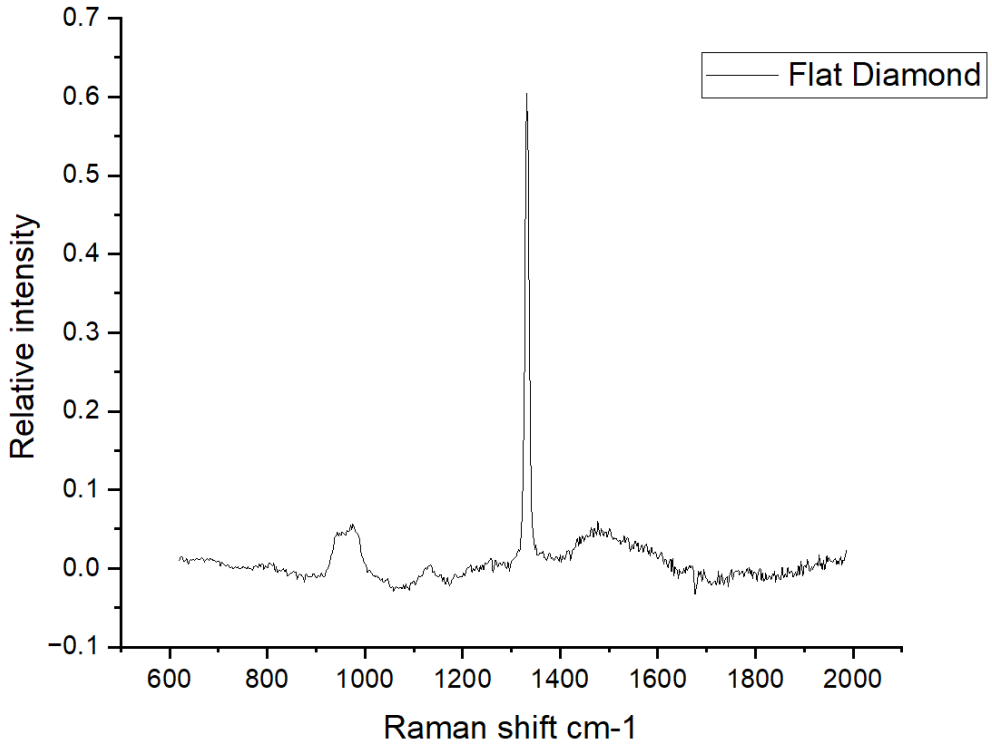

FIGURE 3.3: Flat diamond Raman spectrum

As can be seen above there are several other peaks also found in the diamond samples. The presence of graphite on the sample is indicated by the series of broad peaks in the range of 1300 to 1500cm^{-1}. This is common to be found on synthetic micro and nanocrystalline diamond surfaces. Within nanocrystalline diamond, according to the literature, there can be found disordered graphite which causes a peak at 1355 cm^{-1} and a peak is found in the 1500 cm^{-1} range.[70] These are known as D and G bands and are due to sp^2 carbons. The peak at 1100c m^{-1} only appears in nanocrystalline diamond structures. A study was completed by Pfeiffer et al to investigate the source of this peak and it was concluded that it was due to trans-polyacetylene, which is present in all diamond grain boundaries but its Raman peak is only usually visible when there are many grain boundaries, such as when there is a nanocrystalline film.[71]

XPS

XPS was a useful technique to check for the presence of carbon in the samples to ensure that diamond had been grown. Both flat and black diamond samples were tested, with two analyses being done, one charge neutralised and one not charge neutralised. Within each run for flat diamond a range of angles were used so as to view the thickness of the layers, and the 1s carbon transition was specifically studied. Over the range of angles that were used, for both charge neutralised and not charge neutralised samples, carbon was confirmed in each sample. The initial survey of both flat and black diamond demonstrated a range of peaks. Below figures 3.4 and 3.5 show the initial surveys for flat diamond and black diamond.

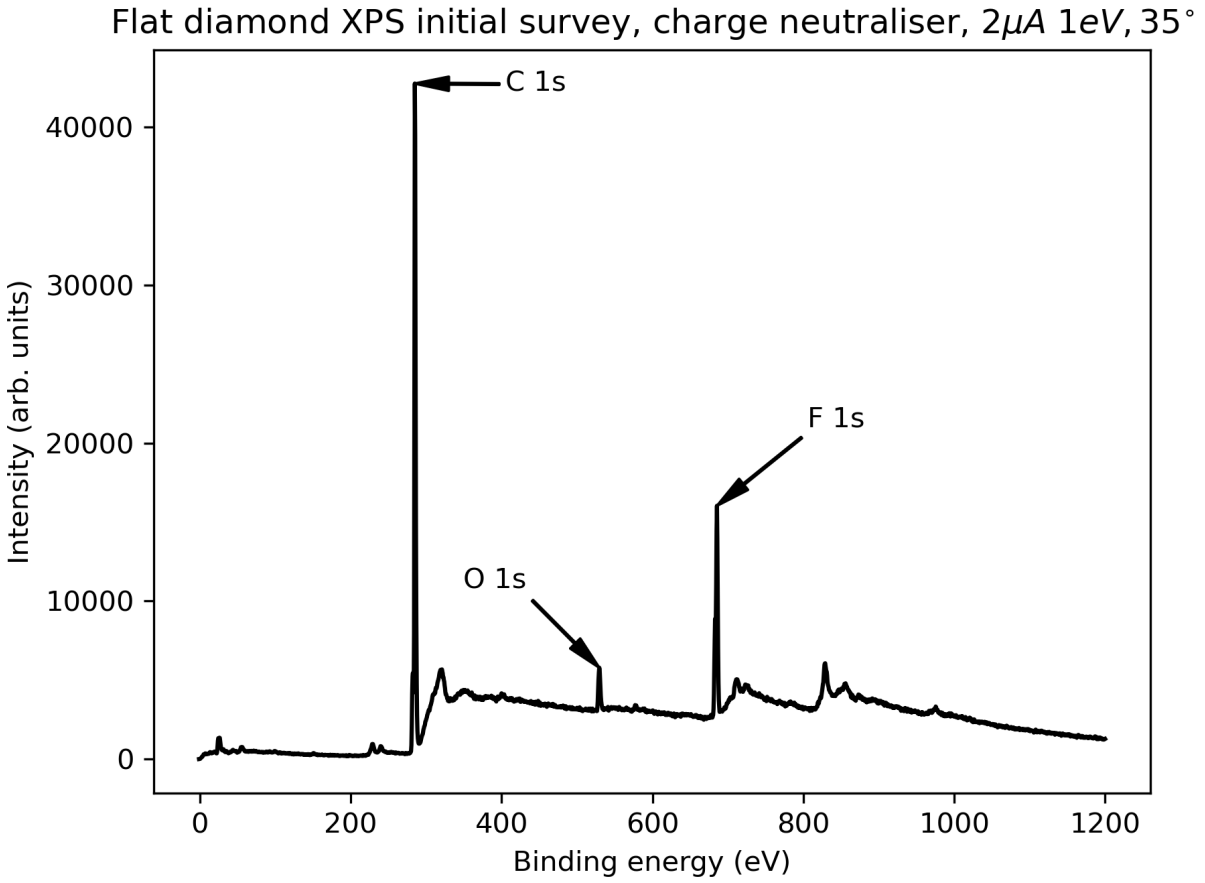

FIGURE 3.4: Initial survey XPS spectrum of flat diamond, charge neutraliser 2 µA, 1 eV, emission angle 35°

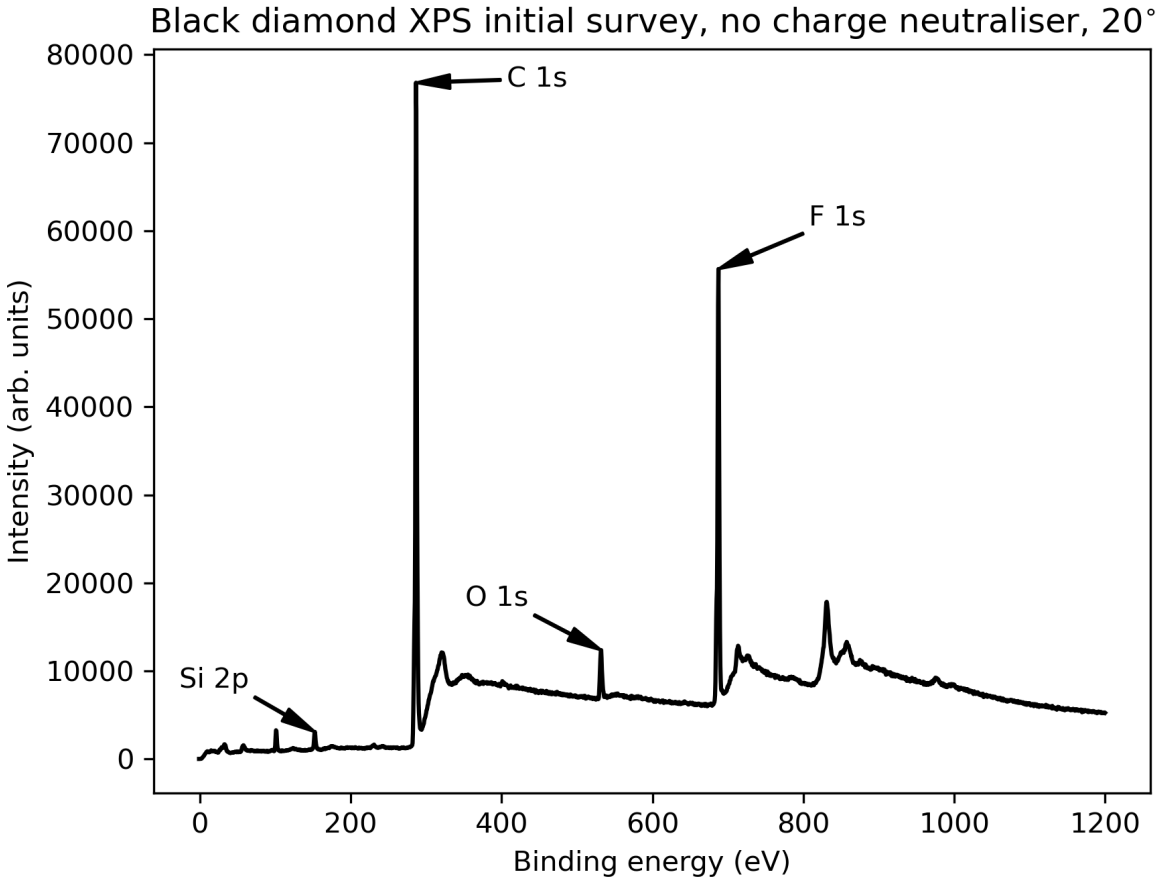

FIGURE 3.5: Initial survey XPS spectrum of black diamond, no charge neutraliser, emission angle 20°

Peak	**Experimental binding energy** */eV*	**Literature binding energy** */eV*	**Peak area** / μm^2
C 1s	286.7	285.2	237913.4
F 1s	687.4	691.2	143920.9
Si 2s	152.2	151.0	7859.789
O 1s	531.9	533.2	53184.07

TABLE 3.1: XPS peak data from initial survey of black diamond, fluorine terminated. Showing presence of carbon, fluorine, silicon and oxygen as expected, with carbon being the most abundant element[62]

From these initial surveys, specific transitions were then looked for, primarily the carbon 1s transition. According to the literature, the binding energy for an sp^3 carbon 1s transition is 285.2 eV.[72] Below in figure 3.6 the carbon presence in a non-charge-neutralised black diamond samples is demonstrated by the 1s transition, with a peak at the binding energy of 286.7 eV, sufficiently close enough to the literature value.

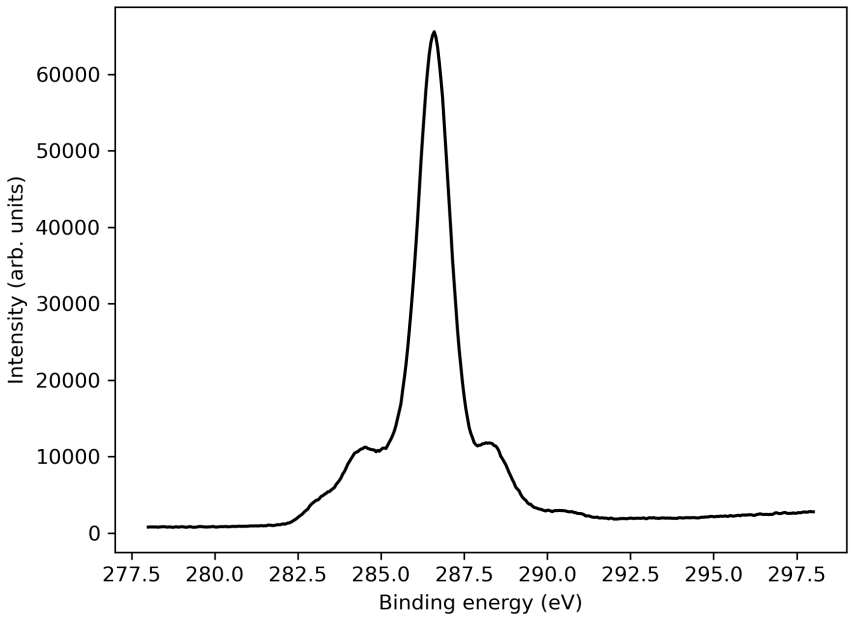

FIGURE 3.6: XPS spectrum of bD showing C 1s transition, no charge neutraliser, emission angle = 20°

The XPS data were also taken at a range of angles on the flat diamond sample to test the depth of the carbon. It was found that the carbon coating seemed to be smooth and cohesive over the sample surface as there was little variation in intensity of the peaks. As can be seen below in figures 3.7 and 3.8, which are runs taken at 5° and 10° angles.

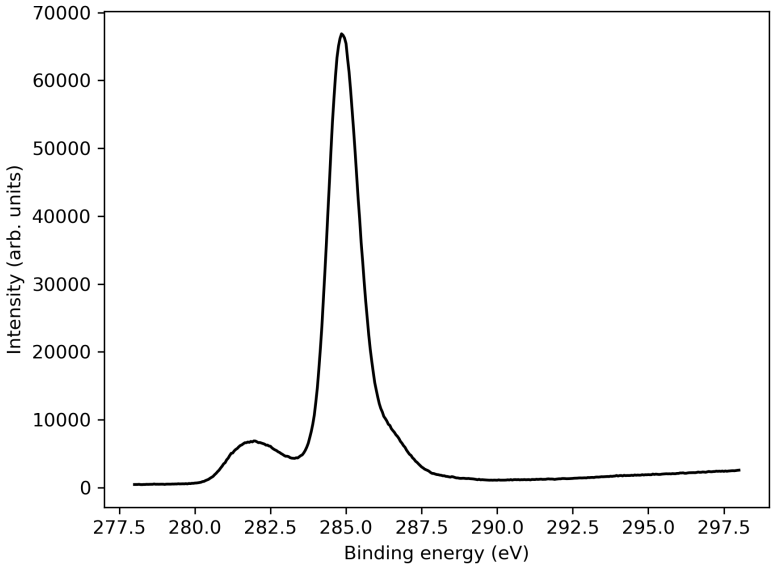

FIGURE 3.7: XPS spectrum of flat diamond showing C 1s transition, no charge neutraliser, 5° angle

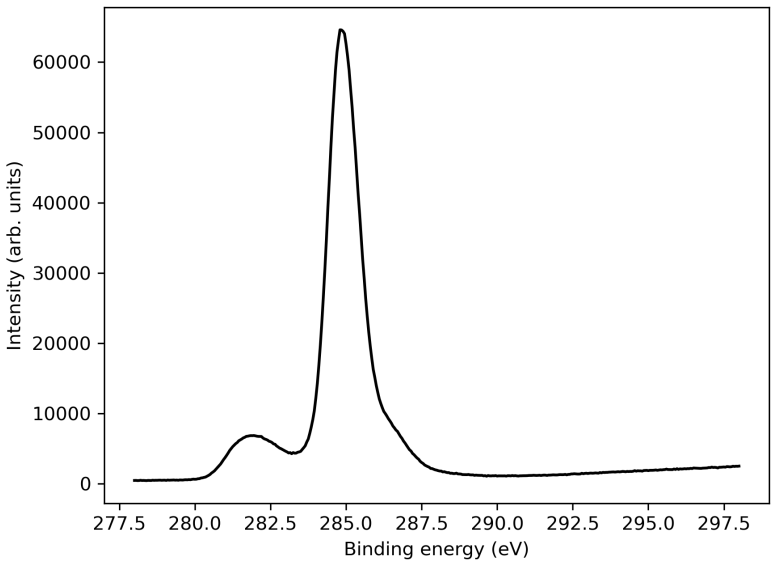

FIGURE 3.8: XPS spectrum of flat diamond showing C 1s transition, no charge neutraliser, 10° angle

There is very little variation between the intensities of the carbon 1s transition peak with the change of emission degree. This implies that there is good continuous surface coverage by the diamond. It should also be noted that very little difference was seen between samples that were charge neutralised and not.

3.1.2 Success of termination

Hydrophobicity of the surfaces of the samples was achieved through fluorine termination. The black diamond was terminated successfully with ease, using a 7 second time period. The success of the termination was verified by two methods: XPS and sessile drop measurement.

XPS

XPS was data was used to confirm the presence of fluorine, and its coverage signified by the intensity of the relevant peak in the spectrum. The range of angles used for analysis all gave similar positive results with a peak at 687 demonstrating the F 1s transition, as shown below in figure 3.9 for the 5°charge neutralised run.

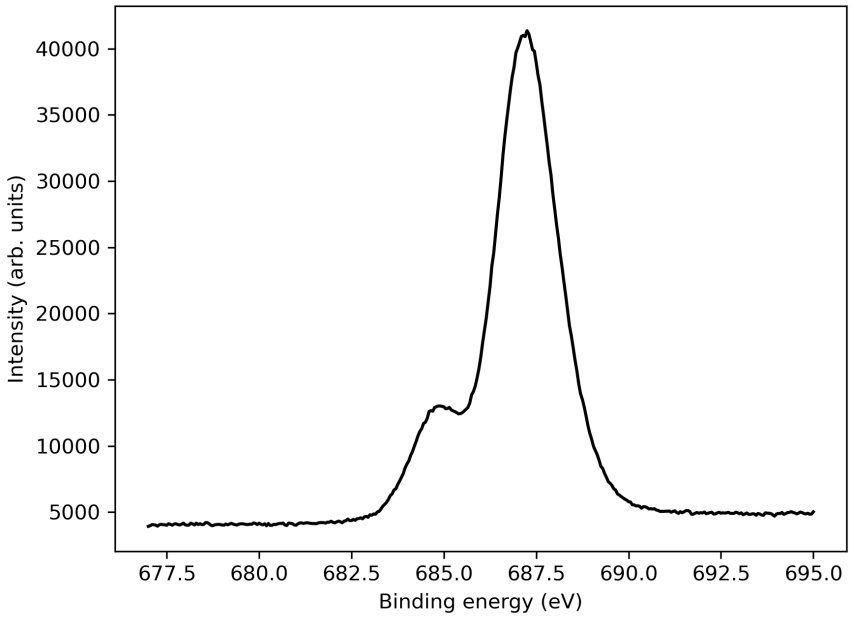

FIGURE 3.9: XPS spectrum of bD showing F 1s transition, no charge neutraliser, 20°

Sessile Drop Measurement

The effectiveness of the fluorine termination was also checked through assessing the hydrophobicity of the sample surface using sessile drop measurement. For black diamond, the water contact angle was found to be greater than 90° in all of the measurements, showing that the surface had been successfully terminated to be hydrophobic, as shown below in figure 3.10. It was found that the longer the diamond was grown for, the greater degree of hydrophobicity was achieved, due to the more prominent needles being formed.

FIGURE 3.10: Black diamond 30 minute growth time fluorine terminated sessile drop contact angle

However, greater difficulty was had in terminating black silicon as termination was unsuccessful multiple times. There were several terminated black silicon surfaces that were shown to be not hydrophobic at all. This is likely because silicon reacts with oxygen in the air forming silicon dioxide and so the F-terminated surface cannot stay hydrophobic very long. In the end it worked successfully with a termination time period of 5 seconds, shown below in figure 3.11.

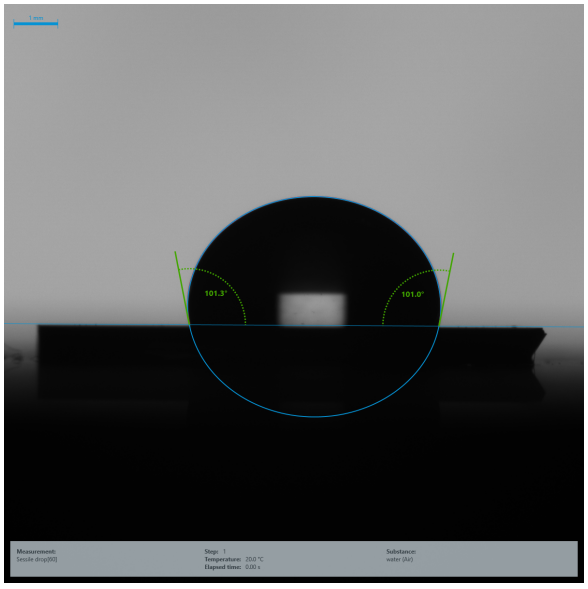

FIGURE 3.11: Black silicon fluorine terminated, water contact angle measurement on KRUSS sessile drop

The samples that were tested on the KRUSS machine had to be fresh so as to prevent the reaction with the air. Although hydrophobicity decreased rapidly with time and so the drop lost its shape after ten minutes on the surface.

3.1.3 Nanostructures of the surfaces

The nanostructures of the surfaces were imaged using SEM. This confirmed that the black silicon had the desired nanoneedle structure, and consequently that the black diamond grown mimicked this spiked structure. In addition to this, flat silicon was used as a surface to grow diamond on as a comparison. Figures 3.12 and 3.13 below show top views of each of black silicon and black diamond surfaces, immediately demonstrating the evident physical differences in the nature of the nanoneedles between them.

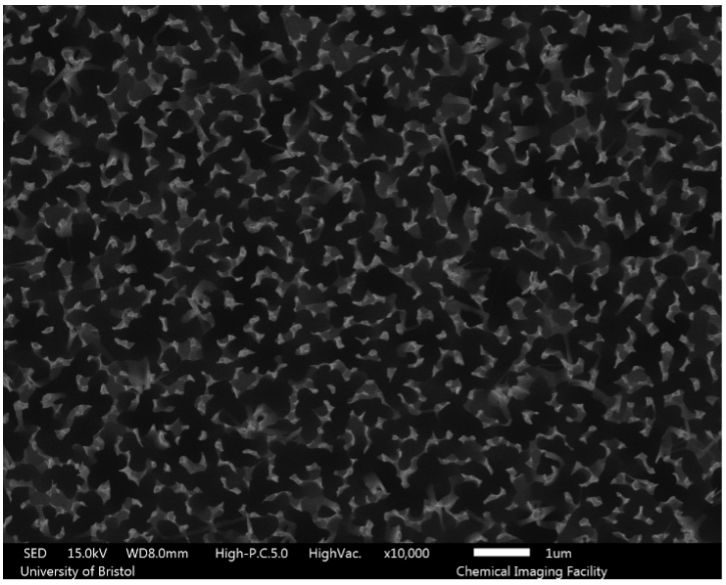

FIGURE 3.12: Black silicon SEM top view

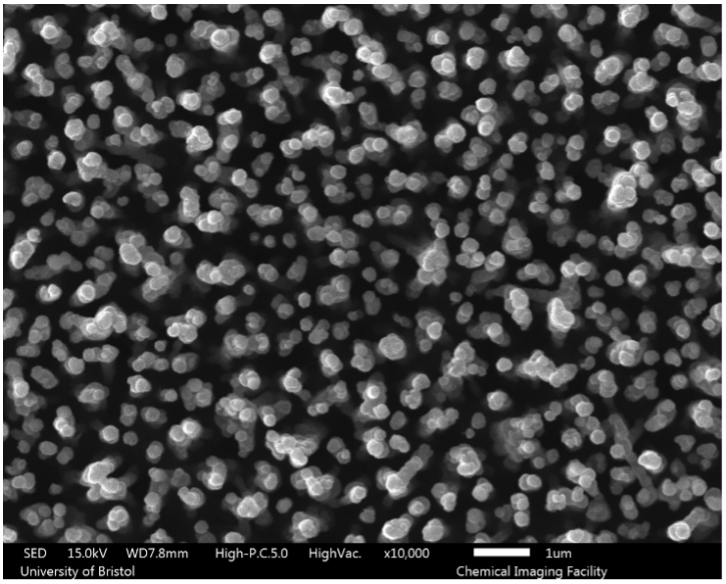

FIGURE 3.13: Black diamond top SEM view

Figures 3.14 and 3.15 below show the starting material of black silicon, unseeded. This is as expected for black silicon. It is extremely fragile and so slight breakages of the spikes can be seen in the 10000× magnification image.

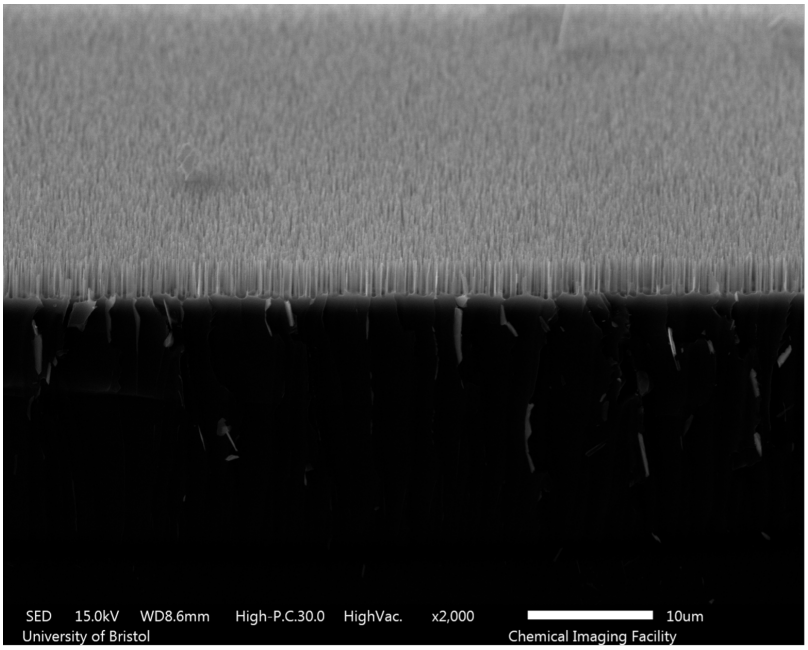

FIGURE 3.14: Black silicon 2000× maginification

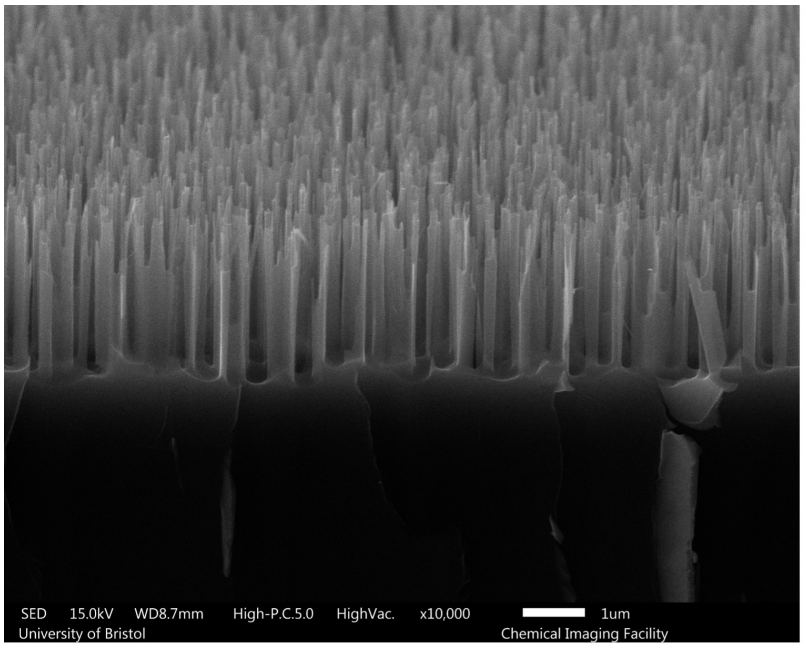

FIGURE 3.15: Black silicon 10000× magnification

The above black silicon was used as the seeded substrate on which to grow black diamond. As can be seen in figures 3.16 and 3.17, the black diamond grown had needles of greater diameter and height than the black silicon. This is due to the thickness that the diamond layer adds to the surface. The black diamond samples were grown over a time period of 30 minutes.

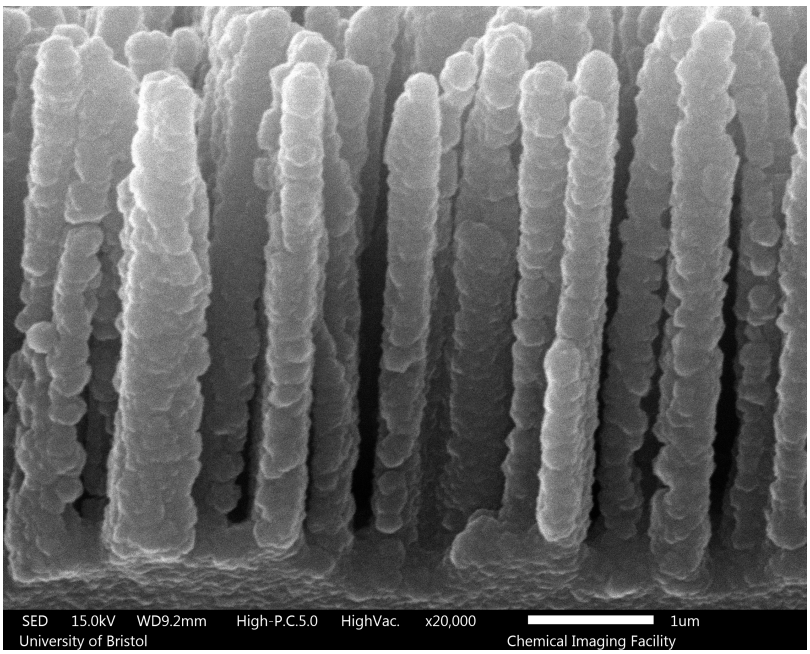

FIGURE 3.16: Black diamond 20000× magnification

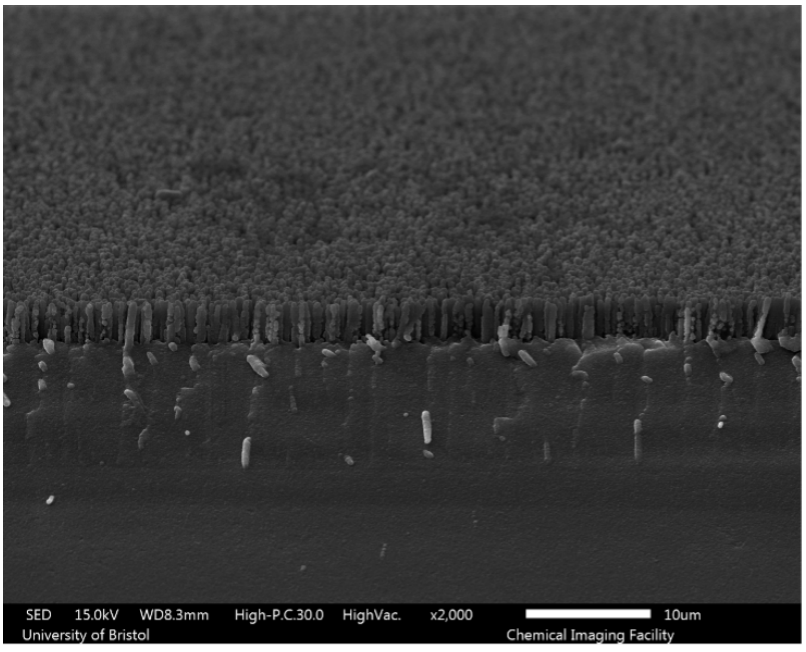

FIGURE 3.17: Black diamond 2000× magnification

For contrast and comparison, diamond was also grown on flat silicon surfaces to examine the difference in resulting structure. As seen below in the SEM images of the diamond grown on the flat silicon for a 6 hour time period, there are no nanoneedles and instead a continuous polycrystalline diamond layer on top of the silicon. This surface structure is shown below in figures 3.18 and 3.19 and has no antimicrobial properties.

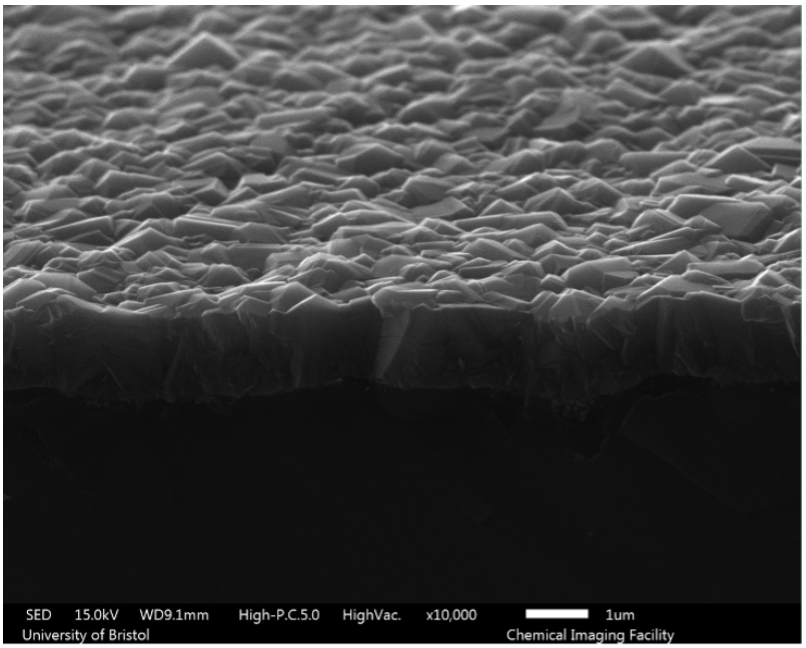

FIGURE 3.18: Flat diamond 10000× magnification

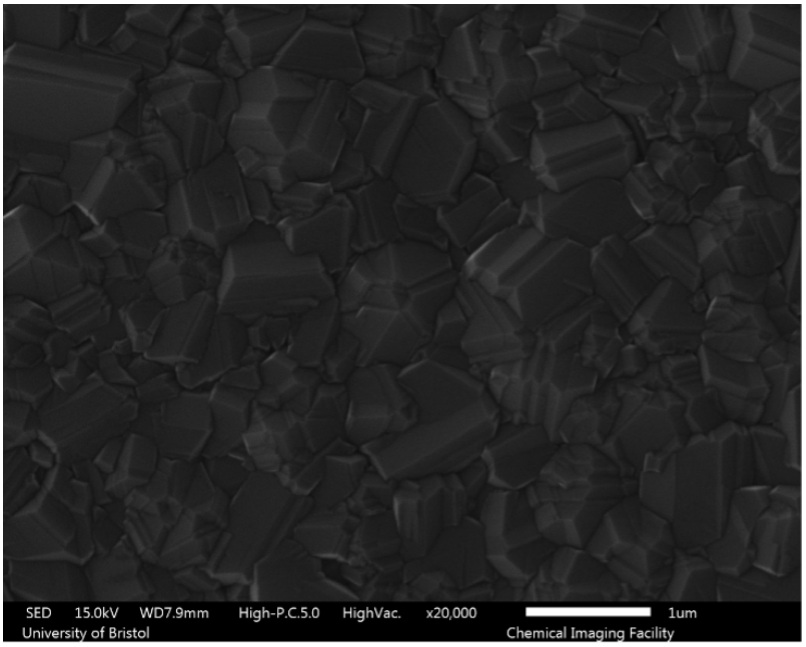

FIGURE 3.19: Flat diamond top view 20000× magnification

3.1.4 Problems with Growth

Several issues arose during the growing process, which was expected as previous investigations into the growth of black diamond have also produced variable results in terms of needle length, diameter and overall coverage.[69] In this case, there was the problem that some of the 30-minute-grown black diamond appeared over grown, with the spikes being rounded and bulging. Comparing these SEM images to those in previous reports shows quite different results.[69] This difference is shown below in figures 3.20 and 3.21.

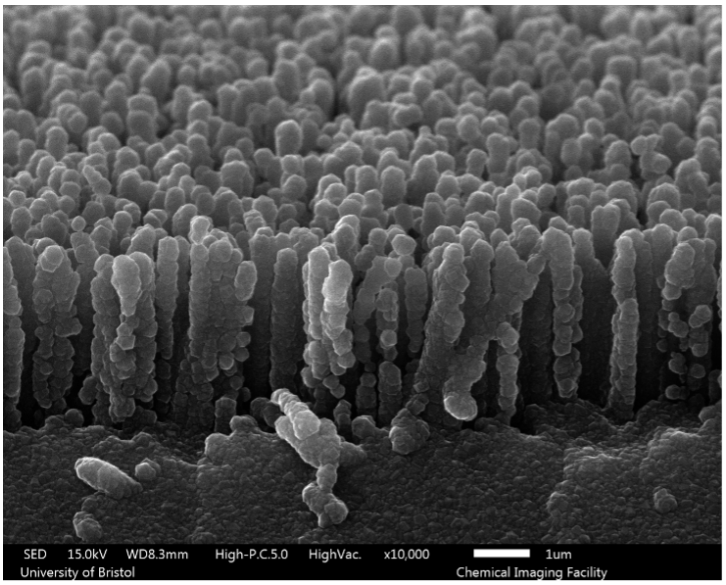

FIGURE 3.20: Black diamond 30 minute growth from this project, overgrown

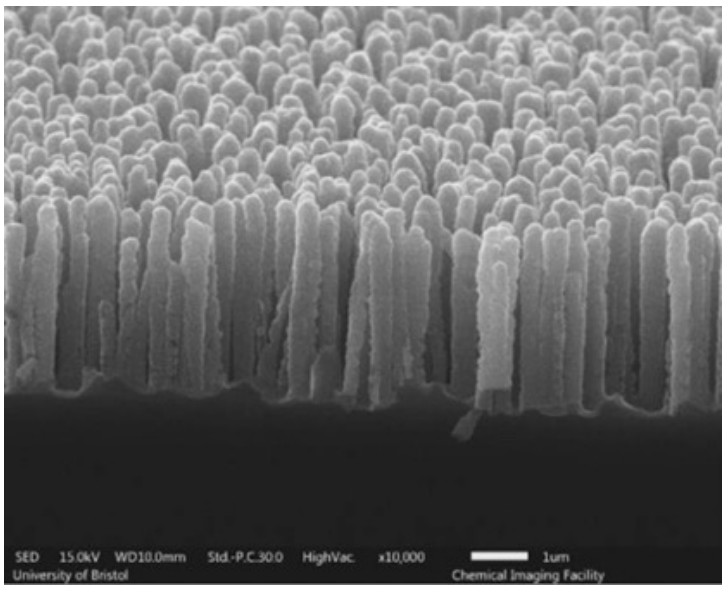

FIGURE 3.21: Black diamond 30 minute growth from different report 2019[69]

In addition to this, several of the samples that were produced showed that only the top half of the black silicon nanoneedles had been coated with the diamond, with the lower half remaining exposed. It is yet to be determined as to why this problem occurred. One hypothesis is that the black silicon substrate may have had a slightly different topography to other studies, that may have

resulted in it being more difficult for the methane radicals to pass through the spikes. This poor coverage is shown below in figure 3.22.

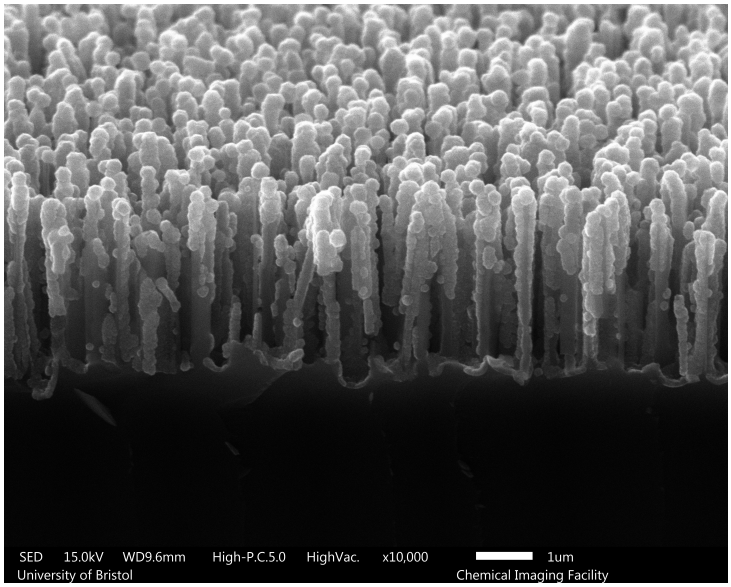

FIGURE 3.22: Black diamond, half coverage, 10000x magnification

This issue was experienced in a more severe state in several other growth runs. In these runs the black diamond barely grew, despite the conditions being the same as previous runs. This lack of growth was evident with the naked eye as the wafers' appearance was still matt black, as opposed to having turned the usual grey colour of black diamond. This was confirmed with SEM imagery showing black silicon with very few specks of diamond on the spikes, shown below in figure 3.23. Again there is no certain explanation for this, but a presumption that the gas flows may have been low or temperatures not as high as required for CVD.

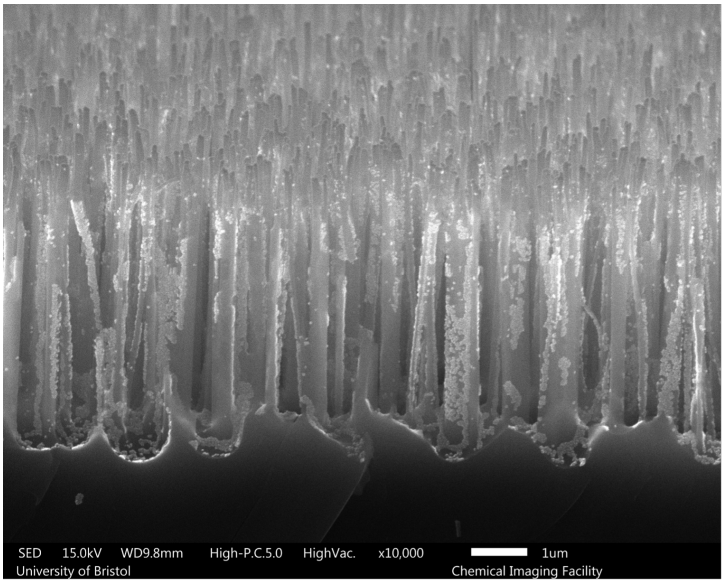

FIGURE 3.23: Black diamond, very poor coverage, 10000x magnification

Despite these issues, a large number of identical black diamond samples were produced during this study, which have been sent to Groningen University to be tested for their effectiveness at killing gram-positive bacteria.

3.2 Polymers

3.2.1 PDMS: Step 1

The PDMS was tested by molding on four different substrate surfaces: black silicon, black diamond, fluorine-terminated black silicon and fluorine-terminated black diamond. For each substrate a range of conditions were attempted, without success, as highlighted in the below table.

Substrate	Room Temperature No antiadhesive	Oven 65 No antiadhesive	Room temperature WD40	Oven 65 WD40
bD	No replication	No replication	Stuck- no result	No replication
bDF-terminated	No replication	No replication	Stuck- no result	-
bSi	Stuck- no result	Stuck- no result	-	-
bSiF-terminated	Stuck- no result	Stuck- no result	-	-

TABLE 3.2: PDMS molding attempts

SEM was used to determine whether the nanotopography of the substrate had been replicated, if at all, in the PDMS. Imaging was carried out on five different samples, none of which showed any replication of the nanoneedles structure. These SEM images are shown below in figures 3.24 - 3.26.

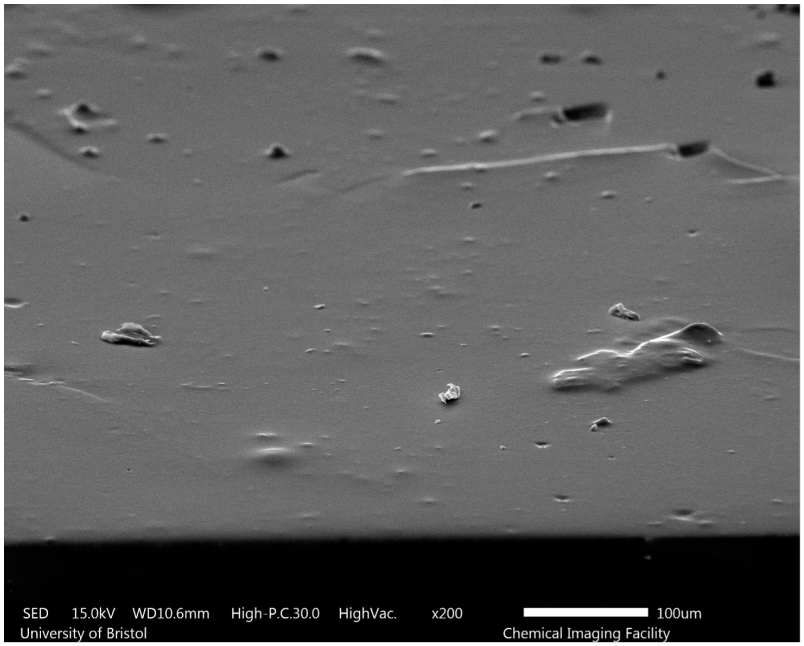

FIGURE 3.24: SEM cross sectional image of PDMS, 10:1 PDMS:curing agent ratio, molded from black diamond fluorine-terminated, cured at 65°C in oven for 2 hours, no anti-adhesive 200× magnification

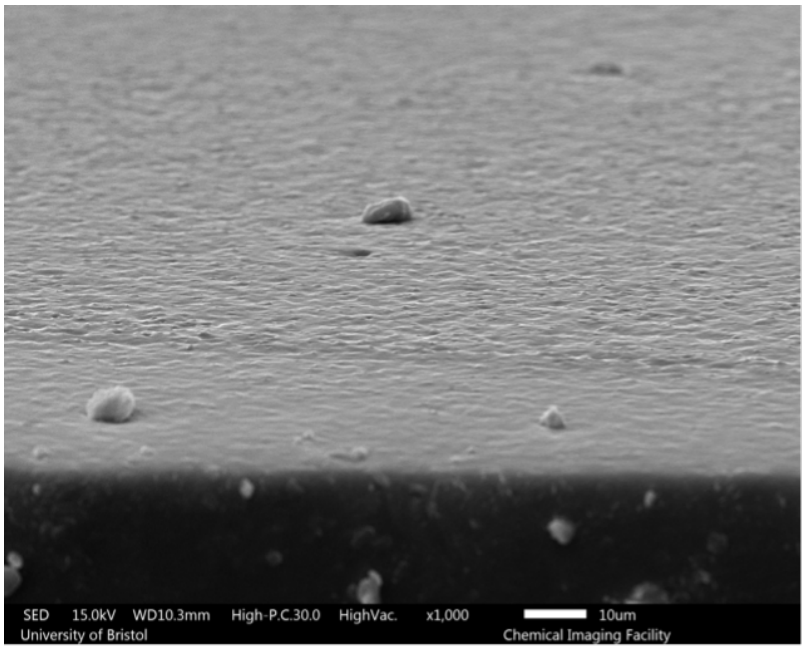

FIGURE 3.25: SEM cross-sectional image of PDMS, 9:1 PDMS:curing agent ratio, molded from black diamond, cured at 65°C in oven for 2 hours, no anti-adhesive 1000× magnification

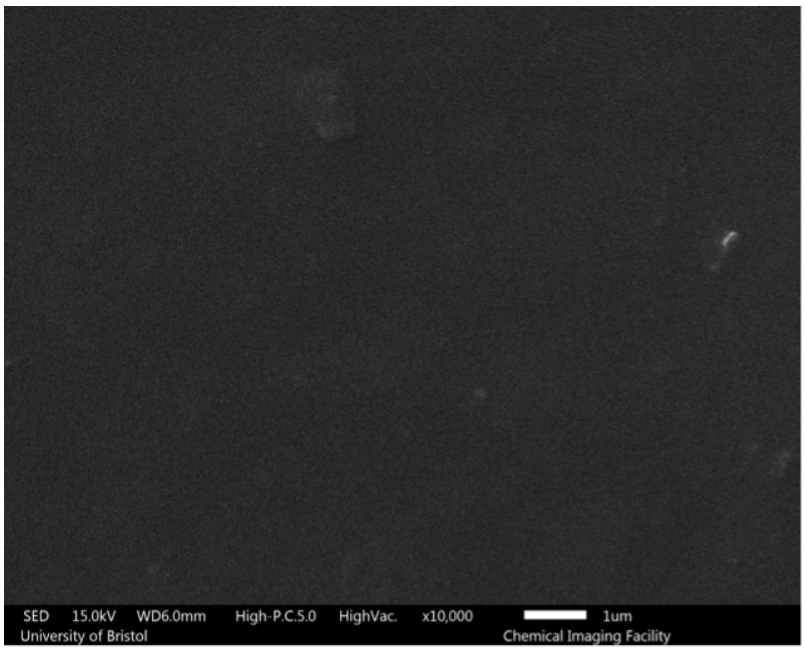

FIGURE 3.26: SEM top view image of PDMS, 9:1 PDMS:curing agent ratio, molded from black diamond, cured at 65°C in oven for 2 hours, no anti-adhesive 10000× magnification

It can be said that the highest degree of success was seen in using 10:1 PDMS:curing agent ratio on a fluorine-terminated black diamond surface and cured at room temperature for 48 hours with no anti-adhesive agent, shown in figure 3.27 below, due to the surface appearing undulating as opposed to entirely flat like in those images above. This suggests that the PDMS molded slightly over the nanoneedles in the black diamond.

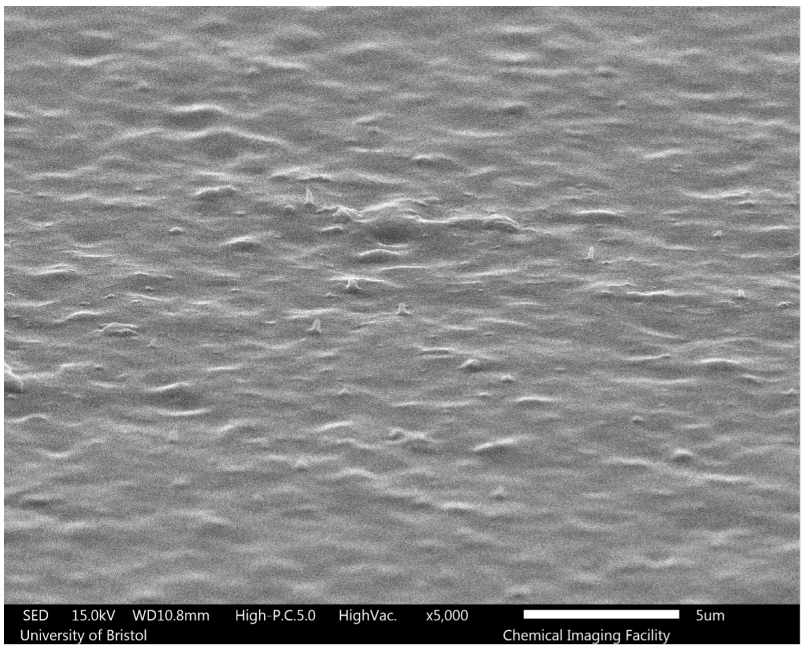

FIGURE 3.27: SEM cross-sectional image of PDMS, 10:1 PDMS:curing agent ratio, molded from black diamond fluorine-terminated, cured at room temperature for 48 hours, no anti-adhesive, 5000× magnification

It is likely that the lack of topographical replication is mainly due to the problems that were had in the peeling off process, as it was difficult to obtain a section of smooth surface that had come off cleanly. This trouble is shown below under SEM imagery as the large gouges in figures 3.28 and 3.29 show that the PDMS had not peeled smoothly off the black diamond. In addition to this, it means that potentially the surface structure was replicated better than the images show, as the peeling off process is likely to have have damaged or left behind any of the structures formed.

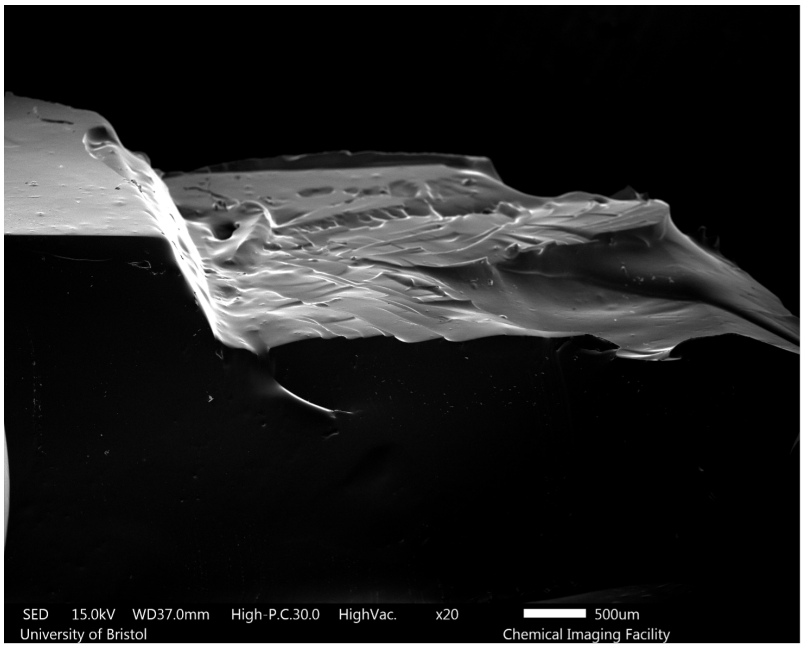

FIGURE 3.28: SEM cross sectional image of PDMS, 9:1 PDMS:curing agent ratio, molded from black diamond, cured at 65°C in oven for 2 hours, WD40 used as an anti adhesive 20× magnification

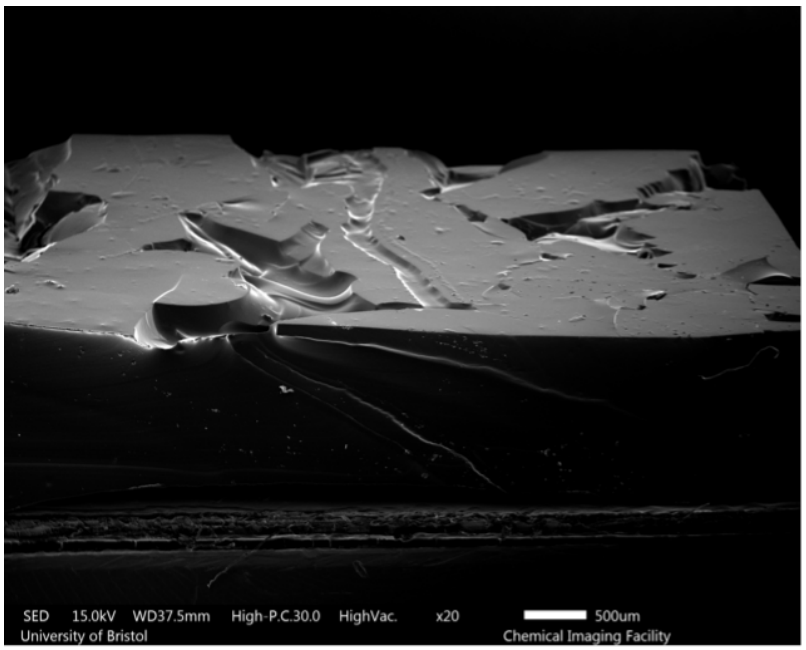

FIGURE 3.29: SEM cross sectional image of PDMS, 10:1 PDMS:curing agent ratio, molded from black diamond fluorine terminated, cured at 65°C in oven for 2 hours, no anti-adhesive 20x magnification

The complete lack of replication may also imply that the PDMS had not managed to penetrate the nanoneedle structure, despite previous studies demonstrating that it had been capable of molding this scale of structures. To assess whether this is the case or not, it will be necessary to carry out several repeats of the experiments so far, whilst also testing out different ways of reducing the adhesion effect. The hydrophobicity has been shown already in this study to be insufficient and so there would be value in pursuing other techniques.

4. Conclusion

Black diamond samples were grown by the process of chemical vapour deposition in a hot filament reactor. With conditions kept constant, the resulting samples were examined and compared, with growth times being varied to assess the difference in coverage between these times. A large number of the desired undamaged 30 minute growth time black diamond samples with good replication of the nanoneedle topography were produced in this project.

However, it was found that despite growth conditions being kept constant, there were still some samples that showed variation in topographies produced, with some having significant variation in the needle coverage by the diamond. The cause of this variation is not known but it is hypothesised that the issues were due to variation in the needle structure of the initial black silicon substrate, and potentially by discrepancies in the seeding process. However, the samples produced that had maintained the nanostructure of the black silicon and had complete coverage were sent off to Groningen University lab in the Netherlands to contribute to continued testing of this surface against gram-positive bacteria, *Staphylococcus aureus* and *Staphylococcus epidermidis*.

The nanoimprinting lithography technique that was used to attempt to create a negative copy of the black diamond using PDMS was not successful in this study. This was mainly due to the experimental preparation being time consuming, as there were complications in obtaining the correct equipment and materials. This led to a lack of time to be able to repeat any tests and solve the problems that were encountered. The main issue faced was the substrates sticking together in the molding process. It is still thought that in the future this technique and material could be very successful, but there are many repeats and changes to the procedure that need to be made to achieve success. Most importantly an effective anti-adhesion layer has to be developed to make sure that the substrate does not stick to the PDMS.

It therefore can be concluded that whilst there remains much to be done in this field of research, this project has shown that black diamond is a reliable antibacterial material that holds potential to be useful to industry. One of the uses has been shown to be as a mold so that its topography can be replicated in a polymer that is cheaper and easier to manufacture. This study has suggested some methods and materials to begin to attempt this strategy, and through research and trials concluded that it will be possible to achieve success.

5. Future Work

Unfortunately, as the first stage of the polymer-molding process proved to be time consuming to prepare for, there was not enough time left to be able to develop the method further. However, with time and repetitions it will be interesting to see whether a good replication of the nanostructure can be achieved. If no success is obtained using PDMS then it will be necessary to explore other polymer options.

Once a successful negative copy of the black diamond has been developed in this first molding step, it will be an exciting field to continue this research through exploring the second stage of the molding process. For this second step, a similar molding and curing technique has been suggested in this report to be used. As outlined above, the polymer TPGDA would be a suitable first material to test out. If this polymer does not work, another option could be found; the main requirements being that it is rigid, UV curable and able to mold to dimensions that fit with the nanospikes.

The presence of an anti-adhesive layer has been shown to be essential to the molding process as sticking will destroy the nanoneedles easily. So a very important aspect of future work in this field will be to find an effective way of reducing adhesion between the molding layers.

With a sufficient amount of time and resources put into the methods proposed in this paper, it is believed that an effective and useful antibacterial surface could be created. Thus taking a step further in the world of fighting bacterial infection, and combatting the issues in this field that are currently faced.

Bibliography

[1] J W Bennett and K.T Chung. Alexander Fleming and the discovery of penicillin. volume 49 of *Advances in Applied Microbiology*, pages 163–184. Academic Press, 2001.

[2] R.J.Fair and Y.Tor. Antibiotics and bacterial resistance in the 21st century. *Perspectives in Medicinal Chemistry*, 6:PMC.S14459, 2014. PMID: 25232278.

[3] P.C Appelbaum. 2012 and beyond: potential for the start of a second pre-antibiotic era? *Journal of Antimicrobial Chemotherapy*, 67(9):2062–2068, 2012.

[4] J Lin, K Nishino, C Roberts, M Tolmasky, I Aminov, and L Zhang. Mechanisms of antibiotic resistance. *Frontiers in microbiology*, 6:34, 2015.

[5] G M S Soares, L C Figueiredo, M Faveri, S Cavalca C, P M Duarte, and M Feres. Mechanisms of action of systemic antibiotics used in periodontal treatment and mechanisms of bacterial resistance to these drugs. *Journal of applied oral science*, 20:295–309, 2012.

[6] J M Munita and C A Arias. Mechanisms of antibiotic resistance. *Microbiology spectrum*, 4(2):4–2, 2016.

[7] *Mutations and selection– Antibiotic Resistance*, React. https://www.reactgroup.org/toolbox/understand/antibiotic-resistance/mutation-and-selection/, 2023. Accessed: 01/03/2023.

[8] H Ceri, E Olson, C Stremick, RR Read, D Morck, and A Buret. The Calgary biofilm device: new technology for rapid determination of antibiotic susceptibilities of bacterial biofilms. *Journal of clinical microbiology*, 37(6):1771–1776, 1999.

[9] M Donlan. Biofilm formation: a clinically relevant microbiological process. *Clinical infectious diseases*, 33(8):1387–1392, 2001.

[10] J Kwiecinski. Biofilm formation by pathogenic *P rototheca* algae. *Letters in applied microbiology*, 61(6):511–517, 2015.

[11] JL Stauber and TM Florence. Mechanism of toxicity of ionic copper and copper complexes to algae. *Marine biology*, 94(4):511–519, 1987.

[12] J Hasan, et al. Selective bactericidal activity of nanopatterned superhydrophobic cicada *Psaltoda claripennis* wing surfaces. *Applied microbiology and biotechnology*, 97(20):9257–9262, 2013.

[13] H J Ensikat, P Ditsche-Kuru, C Neinhuis, and W Barthlott. Superhydrophobicity in perfection: the outstanding properties of the lotus leaf. *Beilstein journal of nanotechnology*, 2(1):152–161, 2011.

[14] J Genzer and K Efimenko. Recent developments in superhydrophobic surfaces and their relevance to marine fouling: a review. *Biofouling*, 22(5):339–360, 2006. PMID: 17110357.

[15] X Zhang, L Wang, and E Levänen. Superhydrophobic surfaces for the reduction of bacterial adhesion. *Rsc Advances*, 3(30):12003–12020, 2013.

[16] S Nishimoto and B Bhushan. Bioinspired self-cleaning surfaces with superhydrophobicity, superoleophobicity, and superhydrophilicity. rsc adv 3: 671–690, 2013.

[17] P Ivanova, et al. Natural bactericidal surfaces: mechanical rupture of *Pseudomonas aeruginosa* cells by cicada wings. *Small*, 8(16):2489–2494, 2012.

[18] Denver P. Linklater, Saulius Juodkazis, and Elena P. Ivanova. Nanofabrication of mechano-bactericidal surfaces. *Nanoscale*, 9:16564–16585, 2017.

[19] E P. Ivanova, et al. Bactericidal activity of black silicon. *Nature Communications*, 4(1):2838, Nov 2013.

[20] M Kelleher, O Habimana, J Lawler, B O'Reilly, S Daniels, E Casey, and A Cowley. Cicada wing surface topography: an investigation into the bactericidal properties of nanostructural features. *ACS applied materials & interfaces*, 8(24):14966–14974, 2016.

[21] S N Kłodzińska, P A Priemel, T Rades, and H M Nielsen. Combining diagnostic methods for antimicrobial susceptibility testing – a comparative approach. *Journal of Microbiological Methods*, 144:177–185, 2018.

[22] C McGoverin, J Robertson, Yb Jonmohamadi, S Swift, and F Vanholsbeeck. Species dependence of syto 9 staining of bacteria. *Frontiers in microbiology*, 11:545419, 2020.

[23] Z A Khan, M F Siddiqui, and S Park. Current and emerging methods of antibiotic susceptibility testing. *Diagnostics*, 9(2):49, 2019.

[24] R Chollet and S Ribault. Use of atp bioluminescence for rapid detection and enumeration of contaminants: The milliflex rapid microbiology detection and enumeration system. In *Bioluminescence-Recent Advances in Oceanic Measurements and Laboratory Applications*. IntechOpen, 2012.

[25] C D. Bandara, S Singh, I O. Afara, A Wolff, T Tesfamichael, K Ostrikov, and A Oloyede. Bactericidal effects of natural nanotopography of dragonfly wing on escherichia coli. *ACS Applied Materials & Interfaces*, 9(8):6746–6760, 2017. PMID: 28139904.

[26] Abinash Tripathy, Prosenjit Sen, Bo Su, and Wuge H. Briscoe. Natural and bioinspired nanostructured bactericidal surfaces. *Advances in Colloid and Interface Science*, 248:85–104, 2017.

[27] S Pogodin et al. Biophysical model of bacterial cell interactions with nanopatterned cicada wing surfaces. *Biophysical Journal*, 104(4):835–840, 2013.

[28] Fudong X, Junjie L, Longfang G, Lirong Z, and Qianzhong L. Theoretical study on the bactericidal nature of nanopatterned surfaces. *Journal of Theoretical Biology*, 385:1–7, 2015.

[29] R Coico. Gram staining. *Current protocols in microbiology*, (1):A–3C, 2006.

[30] S Kumar. *Textbook of microbiology*. JP Medical Ltd, 2012.

[31] J Gumbart. *Simulations of bacterial systems*. https://simbac.gatech.edu/outer-membrane-proteins/, 2012. Accessed: 2023-04-09.

[32] J Jenkins. Winning microscopy images from royal society. *Wiley Analytical Science*, Dec 2017.

[33] C M Bhadra, Vi Khanh T, V TH Pham, M Al Kobaisi, G Seniutinas, J Y Wang, S Juodkazis, R J Crawford, and E P Ivanova. Antibacterial titanium nano-patterned arrays inspired by dragonfly wings. *Scientific reports*, 5(1):1–12, 2015.

[34] N Ziegler, C Sengstock, V Mai, T A Schildhauer, M Köller, and A Ludwig. Glancing-angle deposition of nanostructures on an implant material surface. *Nanomaterials*, 9(1):60, 2019.

[35] J Olmo, L Ruiz-Rubio, L Pérez-Alvarez, V Sáez-Martínez, and J Vilas-Vilela. Antibacterial coatings for improving the performance of biomaterials. *Coatings*, 10(2):139, 2020.

[36] M Cloutier, D Mantovani, and F Rosei. Antibacterial coatings: challenges, perspectives, and opportunities. *Trends in biotechnology*, 33(11):637–652, 2015.

[37] J S Kim et al. Antimicrobial effects of silver nanoparticles. *Nanomedicine: Nanotechnology, Biology and Medicine*, 3(1):95–101, 2007.

[38] DK Luscombe and GP Ellis. *Progress in Medicinal Chemistry. 30*. Elsevier Science Limited, 1993.

[39] F Furno, et al. Silver nanoparticles and polymeric medical devices: A new approach to prevention of infection? *The Journal of antimicrobial chemotherapy*, 54:1019–24, 12 2004.

[40] S Wu, F Zuber, J Brugger, K Maniura-Weber, and Q Ren. Antibacterial Au nanostructured surfaces. *Nanoscale*, 8(5):2620–2625, 2016.

[41] R Stephens and G Cody. Optical reflectance and transmission of a textured surface. *Thin Solid Films*, 45(1):19–29, 1977.

[42] Y Zhang, C Kong, S Davidsen, G Scardera, L Duan, T Khoo, D Payne, B Hoex, and M Abbott. 3d characterisation using plasma fib-sem: A large-area tomography technique for complex surfaces like black silicon. *Ultramicroscopy*, 218:113084, 2020.

[43] H Jansen, M de Boer, R Legtenberg, and M Elwenspoek. The black silicon method: a universal method for determining the parameter setting of a fluorine-based reactive ion etcher in deep silicon trench etching with profile control. *Journal of Micromechanics and Microengineering*, 5(2):115, 1995.

[44] J Lv, T Zhang, P Zhang, Y Zhao, and S Li. Review application of nanostructured black silicon. *Nanoscale research letters*, 13(1):1–10, 2018.

[45] C Hsu, J Wu, Y Lu, J Flood, R Barron, and L Chen. Fabrication and characteristics of black silicon for solar cell applications: An overview. *Materials science in semiconductor processing*, 25:2–17, 2014.

[46] Y Yu, Z Zhang, X Yin, A Kvit, Q Liao, Z Kang, X Yan, Y Zhang, and X Wang. Enhanced photoelectrochemical efficiency and stability using a conformal TiO_2 film on a black silicon photoanode. *Nature Energy*, 2(6):1–7, 2017.

[47] Emmanuel Korawinga Nshingabigwi. *Cross-section Transmission Electron Microscopy of Radiation Damage in Diamond*. PhD thesis, University of the Witwatersrand, 2006.

[48] JJ Gracio, QH Fan, and JC Madaleno. Diamond growth by chemical vapour deposition. *Journal of Physics D: Applied Physics*, 43(37):374017, 2010.

[49] J Angus, H Will, and W Stanko. Growth of diamond seed crystals by vapor deposition. *Journal of Applied Physics*, 39(6):2915–2922, 1968.

[50] W May, P. Diamond thin films: a 21st-century material. *Philosophical Transactions of the Royal Society of London. Series A: Mathematical, Physical and Engineering Sciences*, 358(1766):473–495, 2000.

[51] K Spear and J Dismukes. *Synthetic diamond: emerging CVD science and technology*, volume 25. John Wiley & Sons, 1994.

[52] Gavin Hazell, Paul W May, P Taylor, Angela H Nobbs, CC Welch, and Bo Su. Studies of black silicon and black diamond as materials for antibacterial surfaces. *Biomaterials science*, 6(6):1424–1432, 2018.

[53] G Grass, C Rensing, and M Solioz. Metallic copper as an antimicrobial surface. *Applied and environmental microbiology*, 77(5):1541–1547, 2011.

[54] B Gates, Q Xu, M Stewart, D Ryan, C Willson, and G Whitesides. New approaches to nanofabrication: molding, printing, and other techniques. *Chemical reviews*, 105(4):1171–1196, 2005.

[55] JP Fouassier. An introduction to the basic principles in uv-curing. *Radiation curing in polymer science and technology*, 1:49, 1993.

[56] Z Jia, J Choi, and S Park. Selection of uv-resins for nanostructured molds for thermal-nil. *Nanotechnology*, 29(36):365302, 2018.

[57] T Scharnweber, R Truckenmüller, A Schneider, A Welle, M Reinhardt, and S Giselbrecht. Rapid prototyping of microstructures in polydimethylsiloxane (pdms) by direct uv-lithography. *Lab on a Chip*, 11(7):1368–1371, 2011.

[58] L J Guo. Nanoimprint lithography: methods and material requirements. *Advanced materials*, 19(4):495–513, 2007.

[59] J Chen, Y Zhou, D Wang, F He, V M Rotello, K R Carter, J J Watkins, and S R Nugen. Uv-nanoimprint lithography as a tool to develop flexible microfluidic devices for electrochemical detection. *Lab on a Chip*, 15(14):3086–3094, 2015.

[60] C Schuster, F Reuther, A Kolander, and G Gruetzner. mr-nil 6000lt–epoxy-based curing resist for combined thermal and uv nanoimprint lithography below 50° c. *Microelectronic engineering*, 86(4-6):722–725, 2009.

[61] CT Pan, TL Yang, CH Chao, ZK Wang, and PR Ni. Study on anti-adhesion layers using afm for nanoimprint process. In *Key Engineering Materials*, volume 661, pages 128–133. Trans Tech Publ, 2015.

[62] ZW Zhong, XC Shan, and YC Yao. Investigation of antiadhesive coatings for nanoimprinting lithography. *Materials and Manufacturing Processes*, 25(7):658–664, 2010.

[63] FA Houle, CT Rettner, DC Miller, and R Sooriyakumaran. Antiadhesion considerations for uv nanoimprint lithography. *Applied Physics Letters*, 90(21):213103, 2007.

[64] A Francone. *Materials and anti-adhesive issues in UV-NIL*. PhD thesis, Institut National Polytechnique de Grenoble-INPG, 2010.

[65] M Schvartzman and S J Wind. Plasma fluorination of diamond-like carbon surfaces: mechanism and application to nanoimprint lithography. *Nanotechnology*, 20(14):145306, mar 2009.

[66] RS Butter, DR Waterman, AH Lettington, RT Ramos, and EJ Fordham. Production and wetting properties of fluorinated diamond-like carbon coatings. *Thin Solid Films*, 311(1-2):107–113, 1997.

[67] K Khanafer, A Duprey, M Schlicht, and R Berguer. Effects of strain rate, mixing ratio, and stress–strain definition on the mechanical behavior of the polydimethylsiloxane (pdms) material as related to its biological applications. *Biomedical microdevices*, 11:503–508, 2009.

[68] Igor Iatsunskyi, Stefan Jurga, Valentyn Smyntyna, Mykolai Pavlenko, Valeriy Myndrul, and Anastasia Zaleska. Raman spectroscopy of nanostructured silicon fabricated by metal-assisted chemical etching. In *Optical Micro-and Nanometrology V*, volume 9132, pages 323–329. SPIE, 2014.

[69] P W May. Production of black diamond by chemical vapour deposition for testing as an antimicrobial surface. *School of Chemistry, University of Bristol*, 2022.

[70] R Haubner and M Rudigier. Raman characterisation of diamond coatings using different laser wavelengths. *Physics Procedia*, 46:71–78, 2013.

[71] R Pfeiffer, H Kuzmany, P Knoll, S Bokova, N Salk, and B Günther. Evidence for trans-polyacetylene in nano-crystalline diamond films. *Diamond and Related Materials*, 12(3-7):268–271, 2003.

[72] P Mérel, M Tabbal, M Chaker, S Moisa, and J Margot. Direct evaluation of the sp^3 content in diamond-like-carbon films by XPS. *Applied Surface Science*, 136(1):105–110, 1998.